TALLINN UNIVERSITY OF TECHNOLOGY
SCHOOL OF ENGINEERING

Department of Materials and Environmental Technology

HYBRID SOLAR CELLS PREPARED BY SELECTIVE PHOTOELECTROCHEMICAL DEPOSITION OF POLYPYRROLE ONTO AMORPHOUS SILICON

Master Thesis

Denisa Dosenovicova

Student code 156323KAYM

Supervisors Dr. Sergei Bereznev

MSc Jelena Maricheva

Tallinn 2017

AUTHOR'S DECLARATION

Hereby I declare, that I have written this thesis independently.
No academic degree has been applied for based on this material.
All works, major viewpoints and data of the other authors used in this thesis have been referenced.

" 30 " May 2017

Author: Dosenovicova
/signature /

Thesis is in accordance with terms and requirements

"....." 2017

Supervisor: ….....
/signature/

Accepted for defence

"....."....."2017

Chairman of theses defence commission: .....
/name and signature/

TALLINNA TEHNIKAÜLIKOOL
INSENERITEADUSKOND

Materjali ja keskkonnatehnoloogia instituut

POLÜPÜROOLI FOTOELEKTROKEEMILINE SADESTAMINE AMORFSE RÄNI HÜBRIIDSETE PÄIKESE PATAREIDE VALMISTAMISEKS

MAGISTRITÖÖ

Denisa Dosenovicova

Üliõpilaskood: 156323KAYM

Juhendaja: Dr. Sergei Bereznev

MSc Jelena Maricheva

Tallinn 2017

AUTORIDEKLARATSIOON

Olen koostanud lõputöö iseseisvalt.
Lõputöö alusel ei ole varem kutse- või teaduskraadi või inseneridiplomit taotletud. Kõik töö koostamisel kasutatud teiste autorite tööd, olulised seisukohad, kirjandusallikatest ja mujalt pärinevad andmed on viidatud.

“ 30 ” May 2017

Autor: Dosenovicova

/ allkiri /

Töö vastab bakalaureusetöö/magistritööle esitatud nõuetele

“.....” 2017

Juhendaja: .....

/ allkiri /

Kaitsmisele lubatud

“.....”.....2017

Kaitsmiskomisjoni esimees .....

/ nimi ja allkiri /

Table of Contents

Acknowledgments

This research was supported by the institutional research funding IUT19-28, University Base finance B54 of the Estonian Ministry of Education and Research, the European Union through the European Regional Development Fund, Project TK141, and by ERA.NET RUS PLUS Project Flexapp (ETAG15028).

I would like to express my sincere gratitude to my supervisors Dr. Sergei Bereznev and MSc Jelena Maricheva for their continuous support, their patience, motivation, enthusiasm, and immense knowledge. Their guidance, kindness and professional approach helped me in all the time of research and writing of this thesis.

I would like to thank Prof. Andres Öpik, Dr. Malle Krunks, Dr. Marit Kauk-Kuusik and Prof. Enn Mellikov for providing an excellent opportunity to carry out my studies and research at the Department of Materials and Environmental Technology.

I would like to thank Prof. Dieter Meissner and Dr. Jaak Kikas for providing a great motivation and inspiration during my master studies.

In addition, I would like to thank everybody whom I worked with in the Department of Material and Environmental Technology, particularly to Dr. Taavi Raadik, Dr. Revathi Naidu and Dr. Natalia Maticiuc for their help in different areas of my studies.

I am grateful to all the people who helped and contributed to great ideas and advices, especially to my partner Mattias Malk and my family in Slovakia and Estonia for their support, to close friends for support and patience and to all my colleagues for challenging and exciting debates during my studies in the field of science.

List of abbreviations, acronyms and terminologies

α	Absorption Coefficient
Acetonitrile	AN
AZO	Aluminium doped Zinc Oxide
CB	Conduction band
CE	Counter Electrode
CV	Cyclic Voltammetry
DC	Direct Current
ECP	Electrically Conductive Polymer
ED	Electrodeposition
Ec	Conduction Band Energy
E_F	Fermi Energy
E_G	Band Gap
E_V	Valence Band Energy
E_{pc}	Cathodic Peak Potential
E_{pa}	Anodic Peak Potential
FF	Fill Factor
HOMO	Highest Occupied Molecular Orbital
HVE	High Vacuum Evaporation
h	Planck's constant
I_{sc}	Short Circuit Current
I_{pc}	Cathodic Current
I_{pa}	Anodic Current

LUMO	Lowest Unoccupied Molecular Orbital
η	Efficiency
NGM	Nucleation and Growth Mechanism
NSANa	Naphtalene-1-sulfonic-acid sodium salt
NSA	Naphtalene-1-sulfonic-acid
OSC	Organic Solar Cell
PCE	Photoconversion Efficiency
PEC	Photoelectrochemical
PECVD	Plasma Enhanced Chemical Vapour Deposition
PPy	Polypyrrole
p-TSA	p-toluenesulfonic acid
PV	Photovoltaic
Py	Pyrrole
RE	Reference Electrode
SC	Solar Cell
SCE	Saturated Calomel electrode
T_g	Transition Temperature
ν	Photon Frequency
VB	Valence band
V_{BI}	Built-in Potential
V_{oc}	Open Circuit Voltage
WE	Working Electrode

Introduction

The demand for energy to meet social and economic development as well as improve human welfare and health is ever increasing. Greenhouse gas emissions resulting from the energy services have contributed significantly to the increase of atmospheric greenhouse gas emission concentrations. Most of the observed increase in global average temperature since the mid-20th century is very likely due to the observed increase in anthropogenic greenhouse gas concentrations. Recent data confirm that consumption of fossil fuels accounts for the majority of global anthropogenic greenhouse gas emissions [1].

There are multiple options for lowering greenhouse gas emissions from the energy system while still satisfying the global demand for energy services. One of the possible options is the deployment of sustainable energy systems such as wind turbines, biomass utilization and hydropower stations. Increasing energy demand and global concerns over the anthropogenic climate change have generated also a new research focusing on alternative photovoltaic (PV) structures.

Silicon (Si) solar cells (SCs) has dominated the PV market, due to Si abundance, non-toxicity, high and stable cell efficiencies and its well-established production infrastructure [2]. However, the methods used to manufacture highly efficient SCs based on crystalline Si (c-Si) are costly. Current purification techniques coupled with high temperature and low output manufacturing techniques result in high energy costs that hinder the progress of monocrystalline Si PV. Significant efforts have been focused on the development of cheaper thin-film Si SCs [3-4]. Thin-film a-Si is an alternative to conventional wafer c-Si. Amorphous thin films can be prepared by a variety of methods including vacuum evaporation, cathode sputtering, electrolytic deposition, ion bombardment of single crystal Si, and the glow discharge decomposition of silane [5]. However, the plasma enhanced chemical vapour deposition (PECVD) is currently the method of choice for production of a-Si thin films [6]. a-Si can be deposited on glass [7], metal foil [8], or plastic [9]. The latter two are flexible substrates enabling the "roll-to-roll" manufacturing where all the layers are deposited as the roll is moved through the process zone. Moreover, the optical properties of a-Si are very promising for collecting, harvesting and converting solar energy into electricity [10]. To further reduce cost and to improve SC's efficiency and stability, hybrid SC structures have been proposed.

Hybrid SC structures combine unique properties of the inorganic semiconductor with those of polymeric material such as taking advantage of the beneficial properties of both types of materials e.g. solution processing of electrically conductive polymers (ECPs) and photogenerating properties of inorganic semiconductors [11]. In recent years a large number of studies have been published concerning hybrid SC based on inorganic material and ECP [12-14]. ECPs have gained importance over the past decades due to their wide application in electronic devices such as organic light emitting diodes (OLEDs) [15], SC [16], photodetectors [17], and thin film field effect transistors [18]. Among the most attractive features of ECP are relatively high conductivity, the tunable conductivity, possibility of production through various synthesizing methods [19]. In addition they have simple processing techniques from solution at room temperature for production of large area, light-weight, flexible and therefore cheap devices [20].

Doped PPy is one of the ECPs that has been extensively researched for various applications such as catalyst support for fuel cells, as a material for artificial muscles and in drug delivery systems [21]. The use in hybrid SCs in combination with a-Si has not been, however, addressed significantly. PPy has attractive features such as the ease of processability, high conductivity, and relative chemical and environmental stability [22].

PPy thin film can be produced from a pyrrole (Py) monomer in electrochemical cell by electrodeposition (ED), photoelectrochemical (PEC) deposition, chemical synthesis and by spin casting onto different substrates. So far, only *Inganäs et al*. [23] reported a photo-assisted PPy ED onto a-Si:H yet excluded photoconversion efficiency (PCE) and PV characterization.

Using a-Si;H layer and PPy ECP layer takes advantage of the photogeneration and charge transport properties of a-Si:H and the solution processing and possibility to tune conductivity of PPy [24]. Photo-assisted ED enables to deposit PPy onto exposed photoactive semiconductor surface therefore to avoid possible short-circuits that could form between PPy and front contact.

The PEC deposition of PPy onto a-Si:H presents a potential to fabricate an n-i-p hybrid SC that combines the advantages of the applied materials and a deposition method. In our study the conventional p-type a-Si layer used for n-i-p a-Si based “superstrate” SCs has been replaced by a PPy film to prepare PPy/i-a-Si:H/n-a-Si:H/AZO/glass hybrid SCs. The aim of this research is to develop hybrid SC based on these materials using photoelectrochemical deposition at low applied potentials and short deposition times.

The organization of the thesis is as following:

Chapter I describes up-to date literature review focusing on the science of individual materials used in PPy/i-a-Si:H/n-a-Si:H/AZO/glass hybrid SC as well as the features of n-i-p SC structures. Additionally, hybrid SC structure and device operation as well as current materials are described. Furthermore, the PEC method is described in general and with the focus on PPy with the current up-to-date information. Finally, the scope of the work and the aim of the study are presented.

Chapter II deals with experimental methods used in PEC deposition of Py onto a-Si:H. These include solution preparation, description of the deposition method as well as characterization methods used. General short description of individual characterization methods and their schematics are provided.

Chapter III includes the obtained results, analysis and discussions.

Chapter IV represents conclusions from the obtained results.

Chapter I: Literature review

1.1 Amorphous Silicon

Atomic and electronic structure of hydrogenated amorphous silicon

Atomic structure

Si atoms in amorphous silicon (a-Si) keep the same basic structure as that of c-Si, i.e. each Si atom is connected to other four Si atoms by covalent bonding arranged tetrahedrally as measured by X-ray and other experimental methods [25]. However, the ordered lattice structure of c-Si is absent in a-Si. There are too many constraints on the positions of atoms to keep all bond lengths and angles close to the values demanded by Si chemistry with a non-crystalline structure. To resolve this problem for a-Si, Si-hydrogen bonds are added; i.e. hydrogen passivation. A high percentage of the Si atoms then make covalent bonds with only three Si neighbours; the fourth valence electron of the Si bonds to a hydrogen atom. There are several atomic configurations for the hydrogen in a-Si:H. *Reimer et al.* [26] showed that there are two principal phases evidenced by proton magnetic resonance and they are called the dilute and clustered phase. The dilute phase contains a particular hydrogen atom about 1 nm located from any other hydrogen atom whereas in the clustered phase there are two or more hydrogen atoms in close proximity (Fig. 1.1).

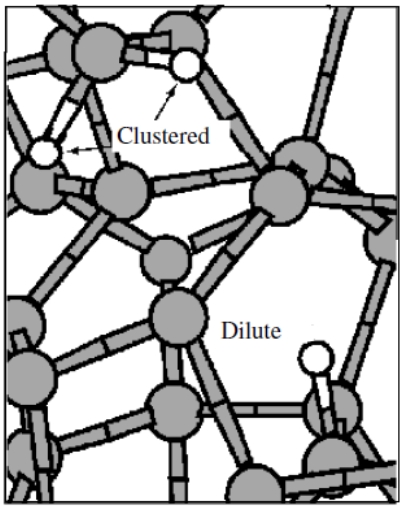

Fig. 1.1. Chemical bonding of a-Si:H with different phase regions [adapted from 27].

Defects in a-Si:H structures

Non-crystalline atomic structure significantly determines general electronic and optical properties of the bulk material. Many electronic properties are affected by the defect of chemical bonding. In a-Si a single type of dangling bonds dominates in experimental measurements, so called D-center defect. As showed by *Jackson et al.* [28] the density of these dangling bonds increases when hydrogen is removed from a-Si:H by heating. Therefore, hydrogen passivation prevents creation of dangling bonds to a certain extend. D-defects themselves are believed to have a smaller impact on PCE; it is rather the light soaking that degrades material's efficiency. One of the limitations of a-Si SCs is the Staebler-Wronski effect [29]. This is enhancement in the defect state density in the material due to a light or current injection; i.e. light soaking. The defect density areas decrease efficiency resulting in SC degradation. The mechanism isn't fully understood but the main understanding is that illumination provides necessary energy to move hydrogen atoms from their diluted phase sites, thus creating D-defect sites. Auspiciously, the light-soaking defects on a-Si cells and ready made films can be removed nearly completely by annealing of a sample at a temperature above 150 °C [30].

Band tails, Band edges, and Band Gap

Any semiconductor has an energy gap between the conduction (CB) and valence band (VB). Ideal crystals have their valence and conduction band-edge energies E_V and E_C well defined, as well as their band gap (E_G): $E_G = E_C - E_V$. In non-crystalline semiconductors there are exponential distributions of band-tail states near these band-edges. Band-tails are trap states that tail off from a high density close to the band edges towards low density further in the band gap. Charge transport is considered as a series of trapping and release actions into a variety of traps with different depths. For the valence band-tail (g_V) which is obtained from the following band tail equation:

$$g(E) = g_V \exp (E - E_V)/ \Delta E_V \qquad (1.1)$$

the width ΔE_V of this exponential distribution is important in order to interpret the optical absorption experiments and for a-Si:H where the typical value of $\Delta E_V = 50 \times 10^{-3}$ eV. ΔE_V also explains the slow drift of holes in an electric field [31]. The conduction band-tail width ΔE_C is much narrower; for the best a-Si:H materials, it is approximately 22×10^{-3} eV, but increases noticeably for doped a-Si as *Wang et al.* [32] confirmed. It is considered that the band-edge is the energy that separates electron orbitals that are localized (those having well-

defined locations in space) from orbitals that are delocalized. The band edges are consequently called the conduction and valence band mobility edges [33].

Unfortunately, for amorphous semiconductors there is no single, well-established procedure for locating the band-edges within the density-of-states. The band gap is therefore problematic to determine without some ambiguity. However, since a-Si–based materials with different band gaps are used in SCs, it is crucial to establish conventional procedures for measuring and comparing the band gaps. The most common approach is to analyse measurements of the optical absorption coefficient α(hν). One typical analysis yields so called "optical" or "Tauc" band gap which can be calculated using equation 1.2:

$$\alpha(h\nu) = (A/h\nu)(h\nu - E_G)^2 \quad (1.2)$$

A- the proportionality constant.

The band gap for a-Si:H obtained using this procedure is typically about 1.75 eV, nonetheless varies considerably with deposition conditions and level of doping. A second simpler procedure is to define the band gap to be the photon energy corresponding to a particular optical absorption coefficient α; using $\alpha = 3 \times 10^3$/cm gives values similar to the Tauc method. Lastly, there is a difference between these optical estimates of the band gap and the real, electrical band gap $E_G = E_C - E_V$. The optical band gap can be defined as the minimum energy required for the photons to be absorbed, while the electrical band gap is the threshold for creating an electron–hole pair that is not bound together (the optical band gap is at a lower energy than the electrical gap) [34]. *Chen et al.* [35] indicated using the internal photoemission measurements that the electrical band gap is 50 to 100 meV larger than the Tauc band gap.

Doping

By doping pure silicon with Group V elements such as P, extra valence electrons are added. These electrons become un-bonded from individual atoms and allow the compound to be an electrically conductive n-type semiconductor. Doping with Group III elements, such as boron (B), creates broken bonds (i.e.holes) in the silicon lattice because these elements miss the fourth valence electron. The result is an electrically conductive p-type semiconductor. Doping is done in order to shift the Fermi energy (E_f) of a particular material. Doped layers are integral to p-i-n SC structures. Doping in a-Si and in c-Si works very differently: in c-Si P atoms substitute silicon atoms in the crystal lattice which is absent in a-Si. P has five valence

electrons and four of them participate in bonding to neighbouring Si atoms. The fifth unpaired electron occupies a state just below the bottom of the conduction band, and the dopant raises the Fermi energy to about this level.

In a-Si, most P atoms bond to only three Si neighbours; they are in threefold coordinated sites. This configuration is advantageous chemically; P atoms normally form only three bonds involving the three valence electrons in the "p" atomic orbitals. The final two electrons paired in "s" atomic orbitals, do not participate in bonding, and remain tightly attached to the P atom. The reason that this more favourable bonding occurs in a-Si, but not in c-Si, is the absence of a rigid lattice. As a thin film of a-Si grows, the network of bonds adjusts to incorporate impurity atoms in a nearly ideal chemical arrangement.

As a comparison, in the c-Si lattice it would be necessary to reorganize a number of Si atoms and to leave a number of dangling Si bonds to accommodate the P atom in this configuration. Therefore, the extra energy for this rearrangement is larger than what would be gained from more ideal bonding of P and substitutional doping is favoured [30].

Occasionally independent formation of both, a positively charged fourfold coordinated P_4^+ and a negatively charged dangling bond D^- arises instead of the more ideal tetrahedral coordination [25]. This leads to two important consequences. Firstly, doping becomes inefficient in a-Si; most dopant atoms do not contribute to creation of a "free" electron and thus do not raise the Fermi energy. Secondly, for every dopant atom that does contribute an electron, there is a Si dangling bond to receive it. These defect levels are located well below the Ec, so the fourfold coordinated P atoms are much less effective in raising the Fermi energy than that in c-Si. Additionally, the negatively charged dangling bonds created by doping act as active traps for holes. Transport of both electrons and holes is essential to photovoltaic energy conversion: photons absorbed in these doped layers will not contribute to the power generated by SCs [30].

To conclude, taking into account the intrinsically defective structure of amorphous semiconductors the addition of monovalent substitutional impurities used in doping crystalline materials does not completely lead to electrically active conditions [36].

Optical properties

The optical properties of a-Si are very promising for collecting solar energy. Fig. 1.2 (a) shows the spectrum for the optical absorption coefficient $\alpha(h\nu)$ for a-Si and c-Si. Fig. 1.2 (b)

shows the spectrum of the integrated solar irradiance intensity (W/m^2) of the solar energy carried by photons above an energy threshold *hv*. An important feature of a-Si:H materials doped with e.g. Ge or C, is that these have direct band gap unlike c-Si. As a consequence, they have at least 100 times higher optical absorption coefficients than the equivalent c-Si. For a-Si:H the very high absorption coefficient allows all incoming light to be collected in 1 μm of material. The significance of this is that only a relatively thin film of a-Si:H is needed to produce an effective device [36]. In comparison with c-Si, to absorb the same energy as the 500 nm thick a-Si:H, the c-Si layer would require much greater thickness. At the same time carriers need to move only 1% as far as in c-Si before they reach a contact. Consequently, the electrical quality of the material may be much lower but carriers can still be collected.

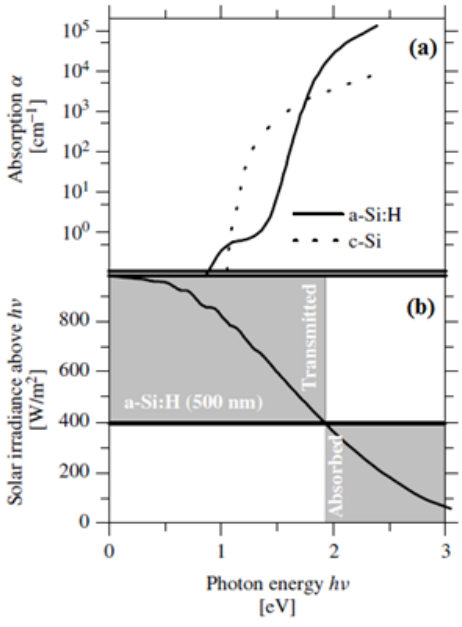

Fig. 1.2. (a) Spectra of the optical absorption coefficient as a function of photon energy (b) the solid curve indicates the irradiance of photons in the solar spectrum with energies hν or larger [30].

The optical properties can vary significantly by changing the deposition condition such as the substrate temperature or dilution of silane by hydrogen atoms in plasma deposition. These changes bring about E_{opt} gap range from 1.6 to 1.8 eV as demonstrated by *Hama et al.* [37]. The different band gaps of a-$Si_{1-x}Ge_x$:H resulting from alloying a-Si:H with different ratio of GeH_4 are shown if Fig. 1.3. The plateau in the absorption coefficient at the lowest photon energies increases gradually as the band gap reduces which corresponds to the increase in the defect density.

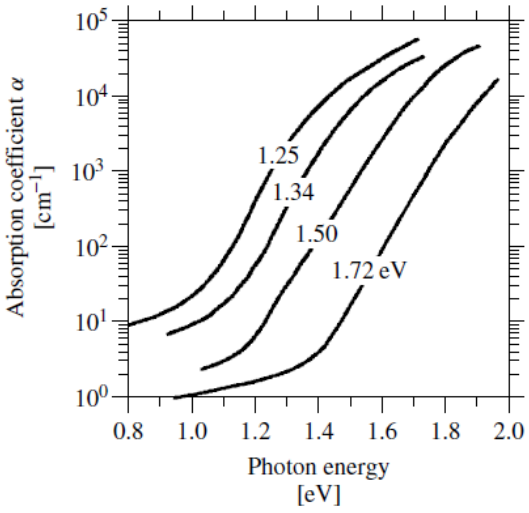

Fig.1.3. Absorption coefficient spectra for a-SiGe alloys; the E_{opts} and corresponding Ge fractions x are 1.25 to 0.58, 1.34 to 0.48, 1.50 to 0.30, 1.72 to 0.0 [38].

Deposition methods for a:Si

The first deposition method ever used was plasma enhanced chemical vapour deposition (PECVD) by *Chittick et al.* [39] but to improve materials quality and deposition rate new methods were subsequently developed. The summary of the most used methods are presented in Table 1.

Table 1.1. Summary of deposition methods for a-Si.

Method	Deposition rate [Å/s]	Advantages	Disadvantages
Radio frequency PECDV	3	High quality, uniform	Slow[40]
Direct Current PECDV	3	High quality, uniform	Slow[41]
Very high frequency PECDV	15	Fast	Poor uniformity[42]
Microwave PECDV	50	Very fast	Poor uniformity[43]
Hot-wire	50	Very fast	Poor uniformity[44]
Photo-CVD	1	High quality	Slow[44]
Sputtering	3	-	Poor quality, slow[46]

Electronic structure of a Si p-i-n photodiode

a-Si can be doped as p-type and n-type, either by mixing Si gas mixture with e.g. B_2H_6 and PH_3, respectively. P doped layers usually act as window layers and therefore need to be transparent. For this purpose a mixture of SiH_4 and CH_4 strongly diluted with hydrogen atoms is usually used [47]. Fig. 1.4 illustrates a band diagram for a p-i-n photodiode.

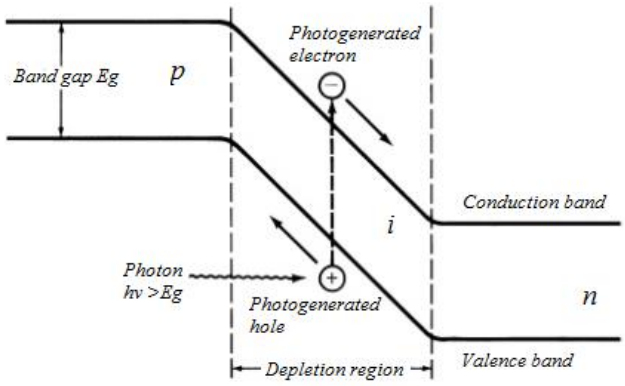

Fig.1.4. A bad diagram for a p-i-n diode.

According to calculations made by *Schrop et al.* individual separated p-type and n-type materials have different E_F [48]. For a-Si:H p-i-n diode E_F is 1.7 eV and 0.05 eV below E_C for the p-layer and n-layer, respectively. When the p-i-n device is constructed, the E_F must be aligned to create thermal equilibrium. Upon merging, electron flow from the n-layer to the p-layer, which eventually creates a built-in electric effect. At the same time, the level positions of E_C and E_V shift across the device; the E_F itself becomes constant. The original difference in Fermi energies becomes the build-in potential (V_{BI}) across the device. Electrons and holes generated by photon absorption drift in the built-in electric field (Fig.1.4.). The design and resulting PCE strongly depends on the rate of electron and hole drift in the electric field. Ideally, photocarriers should drift across the cell without any interaction with each other, the electrons eventually being collected in the n-layer and holes in the p-layer. However, usually a portion of the photocarriers recombines which causes power loss by heat generation [30].

The effect of the thickness of the absorber i-layer

When illuminating from the p-layer, for intrinsic layers that are sufficiently thin, the power is equalled to the number of photons absorbed [30]. In this range the FF has nearly ideal values of approximately 80%. However as the thickness of the cell increases the power saturates. Power saturation occurs for thickness greater than 100 nm which is coincidentally a

typical distance at which the photons are absorbed. Thicker cells will not absorb much additional light, and therefore the power stops to increase above this length (Fig. 1.5.).

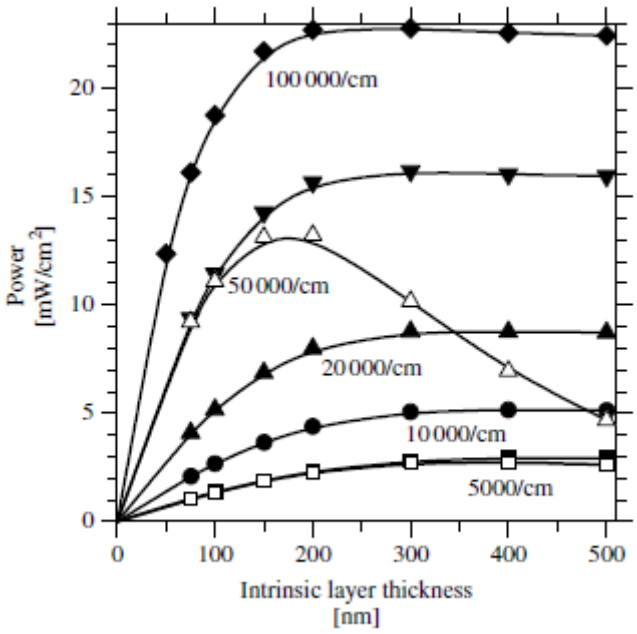

Fig. 1.5. Power output from a p-i-n SC as a function of intrinsic layer thickness [49]. Solid symbols indicate illumination through the p-layer and open symbols indicate illumination through the n-layer.

Weakly absorbed illumination corresponds to photon energy of 1.8 eV. Fig. 1.5 shows there is power saturation when the thickness of the intrinsic layer is about 300 nm. This collection length originates in the region where field breakdowns [48]. The collapsed electric field is stronger near the p-layer and weaker near the n-layer. The recombination of electrons and holes happens largely in the weak field regions. Since electrons and holes are generated at the same rate, their distribution is equal. As a result, they build up under illumination until their rate of recombination with each other matches the rate of photogeneration. There is a certain asymmetry in the hole and electron drifts at different thicknesses of the i-layer when illuminated from either p- or n-layer. This asymmetry also explains better efficiencies achieved when p-i-n a-Si SCs are illuminated through the p-layer.

At weakly absorbed light (5000/cm) the photogeneration of carriers is basically uniform throughout the cell for all the thicknesses shown, and the cell does not show any preferences to n- or p- layer illumination. For more strongly absorbed light entering through the n-layer (50 000/cm) the cells are thinner than the absorption length and the photogeneration is

essentially uniform. Again there is no difference in the power generated for illumination through the n- and p layers [30].

However, for thicker cells, there is a significant decrease in the power generated from the cell illuminated from the n-layer compared to illumination from the p-layer. The power decreases because the holes must drift significantly further to reach the p-layer than when they are generated by illumination from the p-layer. The electric charge of the slowly drifting holes builds up and the electric field breakdowns, eventually leading to recombination power losses.

A-Si in PV Application

SCs are photodiodes which when exposed to light produce an electric current. a-Si:H is one of the most widely manufactured material for thin film SCs because it can be deposited by well-known techniques and cheaply onto either glass, plastic and thin film metal foils. Most a-Si:H SCs are of a p-i-n structure which consists of highly doped p- and n-type regions with an undoped i-layer sandwiched between them (Fig.1.6). I-layer is specifically adjusted for better carrier collection and acts as a photoabsorber [36].

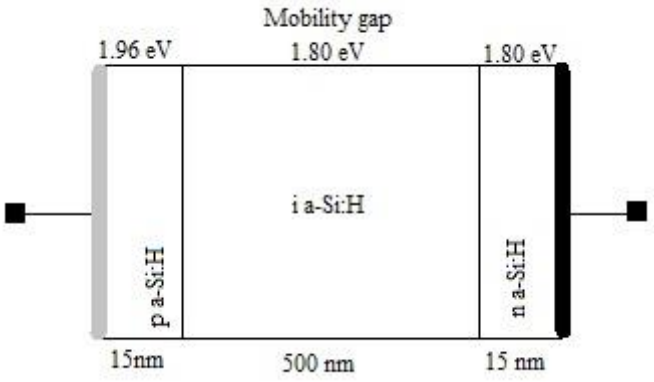

Fig. 1.6. A general a-Si:H SC with an n-i-p structure.

High quality absorber material has fewer defect states in the gap and therefore the built-in electric field moves continuously and uniformly from one contact to another through the absorber layer. This maximizes the field assisting collection of carriers where they are generated and produces the highly efficient SCs [36]. If the density of defects is high the field is localized predominantly near the contacts. Field localization causes several effects: reduced

electric field in the bulk of the i-layer leading to less current generation by the device and in forward bias (i.e. in dark) current injection[1] at the contacts becomes space charge limited [36].

If charge carriers are injected from a contact into a very low mobility material they gather near the contact. Because the mobility is low, they might be unable to further move to the bulk of the low mobility layer as fast as they are injected. This results in a field near the contact which will reject additional injection, eventually increasing the contact resistance at high current levels. High quality materials have relatively high mobilities and carrier diffusivities. Here, space charge limitations become insignificant and the device works well. Conversely, low carrier mobility results in poor carrier collection: the device has low currents and voltages.

The present technology for amorphous SCs involves three diode junctions in series. Each junction collects energy from a sequentially longer wavelength portion of the solar spectrum as light passes from the top to the bottom of the device. Each junction has an increasingly lower mobility gap and is transparent to the light below the mobility gap energy. Any light passing through one deice is available to the next if its energy exceeds the mobility gap energy of that particular material. The current produced by each junction is set by the number of photons in the portion of the solar spectrum that is absorbs and its collection efficiency. The power output is then equalled to current and voltage at a given load.

The progressively lower energy gaps are achieved by two layers deposited with different hydrogen contents and third layer usually consisting of a Si/Ge alloy. Other less common devices are built using a-Si:H only for the wide gap layer with Si/Ge alloys for both narrower gap regions [30].

High-efficiency triple-junction thin-film Si SC using undoped a-Si:H was recently demonstrated stability against light soaking. *Sai et al.* [50] achieved a stabilized efficiency of 14.04% in an a-Si:H/μc-Si:H/μc-Si:H triple-junction SC with a minimum light-induced degradation, setting a new record in this type of SCs.

[1] The current injection technique is a technique developed to reduce the turn-off switching transient of power bipolar semiconductor devices [48].

1.2. Electrically Conductive Polymers (ECPs)

In ECPs SCs, electron donor and electron acceptor materials are involved as opposed to general semiconductor p-n junction type of structure. Usually, organic solar cell (OSC) is composed of an organic PV active layer sandwiched between a transparent front electrode and back metal contact (Fig. 1.7) [51].

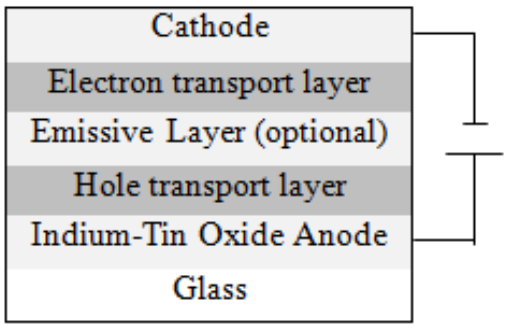

Fig. 1.7. A schematic diagram of a typical organic light-emitting device.

The active layer is composed of a blend conjugated polymer film, which acts as an electron donor, and an acceptor molecule. Conjugated polymers have delocalized electron system which enables them to generate photocurrent upon illumination and transport them to electrodes [52]. Some of the most important hole conducting donor-type semiconducting polymers are poly(3-hexylthiophene) (P3HT), poly(3-octylthiopene) (P3OT), derivatives of phenylene vinylene backbones such as poly[2-methoxy- 5-(3,7-dimethyloctyloxy)]-1,4-phenylenevinylene) (MDMOPPV), and derivatives of fluorene backbones such as (poly(9,9′-dioctylfluorene-co-bis-N,N′-(4- butylphenyl-1,4-phenylenediamine) (PFB) [52]. Conversely, one of the most important electron acceptor is fullerene C_{60} [53].

ECPs can be considered as intrinsic wide band gap semiconductors (band gaps above 1.4 eV) with an insignificantly low intrinsic charge carrier density at room temperature and in the dark. Chemical, photochemical, or electrochemical doping is used to introduce extrinsic charge carriers into organic semiconductors [54]. Doping process significantly influences conductivity of ECPs. Undoped ECPs, such as polythiophenes, polyacetylenes only have a low electrical conductivity of around 10^{-10} to 10^{-8} S/cm. Even very low level of doping (< 1%) increases electrical conductivity significantly by several orders of magnitude up to values of around 0.1 S/cm. Doping of the conducting polymers reaches a saturation point at values around 0.1–10 kS/cm for different polymers [55]. Other factors influencing conductivity

include the orientation, crystallinity and purity of the conjugated polymers [56]. Organic semiconductors have relatively strong absorption coefficients (usually 10^5 cm^{-1}), which partially balances low mobilities, giving high absorption in even <100 nm thin devices [57].

Donor/acceptor type bilayer devices can work like a classical p-n junction semiconductor device. For example, photoinduced electron transfer from a donor to an acceptor-type organic semiconductor film introduces free charge carriers: positive charge carriers on the donor layer, and negative charge carriers on the acceptor layer [58].

Mechanism of conductivity

ECPs are able to transport electric current and to absorb light in the UV part of the solar spectrum due to the sp^2 hybridization of carbon atoms (Fig. 1.8).

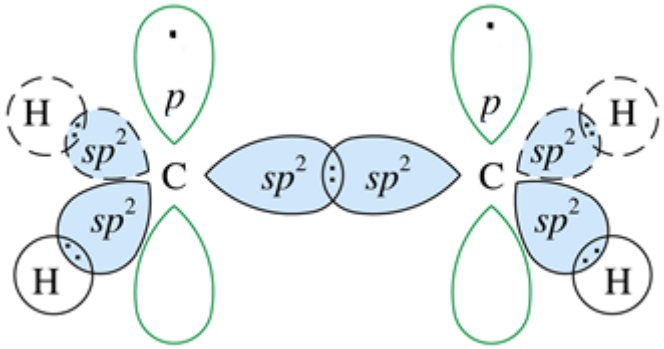

Fig. 1.8. Sp^2 hybridization in ethylene molecule showing delocalized π and π* orbitals (green lobes) containing ‘’free electrons’’ partially responsible for conductivity in ECPs [adapted from 59].

In ECPs the electron in the p_Z orbital of each sp^2 hybridized carbon atom forms bonds with neighbouring p_Z electrons in a linear chain of sp^2 hybridized carbon atoms (Fig. 1.9) which leads then to an alternating single and double bond structure. These electrons have a delocalized nature because of the isomeric effect which results in high electronic polarizability [60].

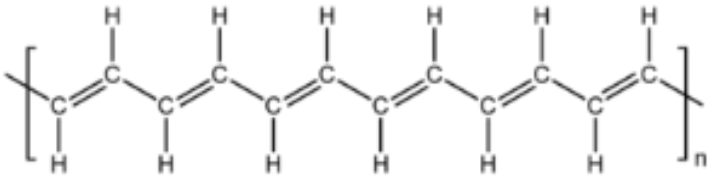

Fig.1.9. A structure of the simplest fully conjugated polymer molecule, trans-polyacetylene, showing alternating single and double bonds.

The sp^2 hybrid orbital forms σ bonds which contain electron pairs in their bonding states and empty anti-bonding states resulting in a very strong covalently bonded molecular backbone. The unhybridized (Fig. 1.8 green orbitals), half-filled p_z, orbitals form the π bonds.

Each carbon atom has a half-filled ”p” state available for π bonding, and therefore the double bonds can be represented as π -bonded molecular orbitals running down the length of the carbon backbone. Additionally, each carbon atom also has one bond left for the attachment of functional groups, usually a hydrogen atom. This availability results in a possibility to add functional groups, making ECPs highly adjustable [36].

However, the simple symmetric structure in linear polymers does not fully account for electron correlation effects. With electron in motion, each electron interacts with all the other electrons, which alter the state energies and exchange one state with another (electron correlation effect) as for example, the lowest unoccupied molecular orbital (LUMO).

According to the quantum mechanical selection rules transitions between states of like-symmetry in a single photon process, where molecules are excited from lower to higher energies, are forbidden. In conjugated backbones the HOMO-LUMO transition change from allowed to disallowed [36,61]. According to *Rockett et al*. [36] the effect is similar to converting an inorganic semiconductor from having a direct band gap to indirect. The optically–active transitions still exist in the conjugated molecule; however, they have no longer the lowest energy transitions (Fig. 1.10).

Both possible transitions that would result from a 1-electron model of the structure and the actual result including electron correlation effects are shown in Fig. 1.10, indicating that the lowest energy optical transitions are not from the HOMO to the LUMO states. Only a two-electron transition is allowed between these states for a single photon process. This is the

main reason why organic semiconductors can behave the same way as do semiconductors with an indirect band gap.

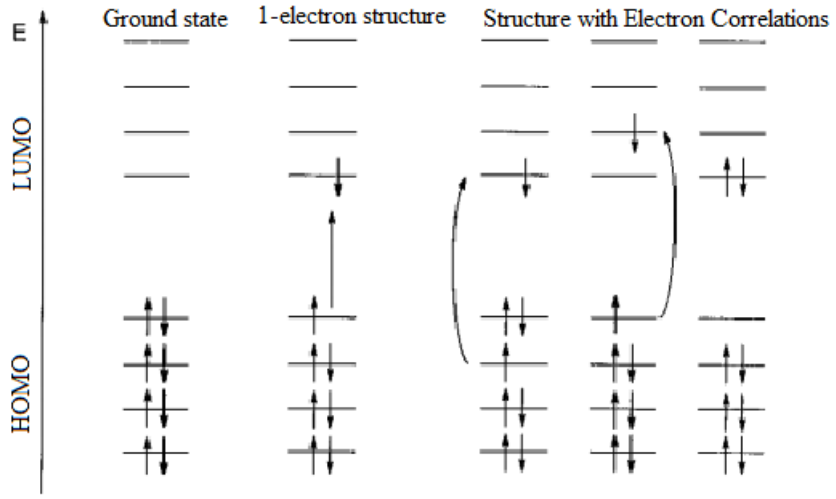

Fig. 1.10. The molecular orbitals for a ECP (trans octatetraene) without hydrogen-carbon bonds and filling of these orbitals with electrons [adapted from 61].

The band of filled or bonding states is called the valence band while the band of empty or anti-bonding states is called the conduction band. Therefore, a free electron in a semiconducting material exists in an anti-bonding LUMO state [62]. Occupying this state eliminates a double bond as both the bonding and anti-bonding states are filled on one atom. This leaves a negative charge on one atom and an unpaired electron on the other. The unpaired electron is known as a soliton [63] or a free radical and is typically distributed over a distance of 1-2 nm on the carbon backbone. Likewise, removing and electron (thus creating a hole) removes one of the electrons forming a double bond and breaks the bond leaving a positive charge behind on one atom and a soliton on the another atom [64]. A soliton travels from one end of the chain to the other by so called hopping mechanism [65] where excitons can carry out hopping motions between adjacent domains [66]. At its simplest, hopping mechanism (i.e. thermally activated tunnelling) is a process by which charge carriers ‘’jump’’ from one monomer to another (in a quantum-mechanical tunnelling process [2]) rather than travelling coherently [67].

[2] Quantum mechanical tunnelling process describes the transition of carriers through a classically forbidden energy state. This can be an electron tunneling from the semiconductor through a dielectric, which represents an energy barrier to the contact. Even if the energy barrier is higher than the electron energy, there is quantum- mechanically a finite probability of this transition. The reason lies in the wavelike behaviour of particles on the quantum scale where the wave function describes the probability of finding an electron at a certain position in space. As the wave function penetrates the barrier and can even extend to the other side, quantum mechanics predict a non-zero probability for an electron to be on the other side [203].

The charged states on molecules can also be considered as the result of oxidation or reduction. The negatively charged atom is called a carbanion and the positively charged atom is a carboacation [68]. Both these can occur on a conjugated molecular backbone. The corresponding electron-hole pair or exciton results from a carbocation lying on a site on the backbone of the molecule adjacent to a carbanion (Fig. 1.11).

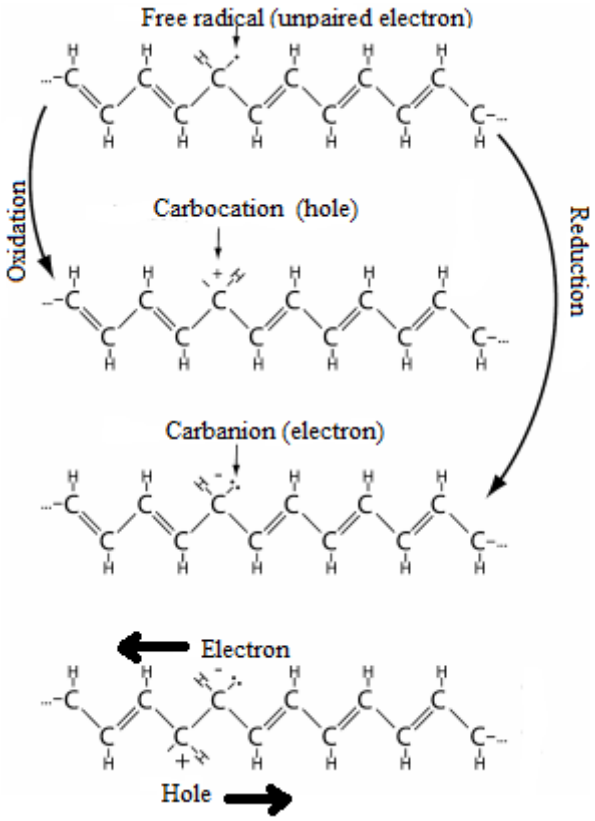

Fig. 1.11. Formation of a free radical, hole, electron and consequent diffusion of a hole-electron pair across the conjugated carbon backbone [adapted from 36].

The conductivity od ECPs can be varied by the symmetry of the conjugated side chain. *Shin et al.* confirmed that the introduction of the symmetric conjugated side chain to the conjugated backbone of the polymer was observed to improve both light harvesting and the charge carrier mobility, by increasing the extent of packing between the polymer chains [69].

Operating Principles of organic solar cells(OSC)

In OSCs donor and acceptor materials are usually in a blend form and have so called dispersed heterojunction (Fig. 1.12. (a)). The light is converted into electricity by the following steps (Fig. 1.12. (b)): a photon absorption leads (1) to the formation of an excited

state (electron-hole pair (exciton) creation); exciton diffuses to a region where exciton separation occurs (2); and charge carriers transport within the organic semiconductor to the corresponding electrodes (3) [70]. For efficient photocurrent generation charge separation should be able to compete with geminate (before exciton separation by diffusion) (4) and interfacial (5) recombination [60].

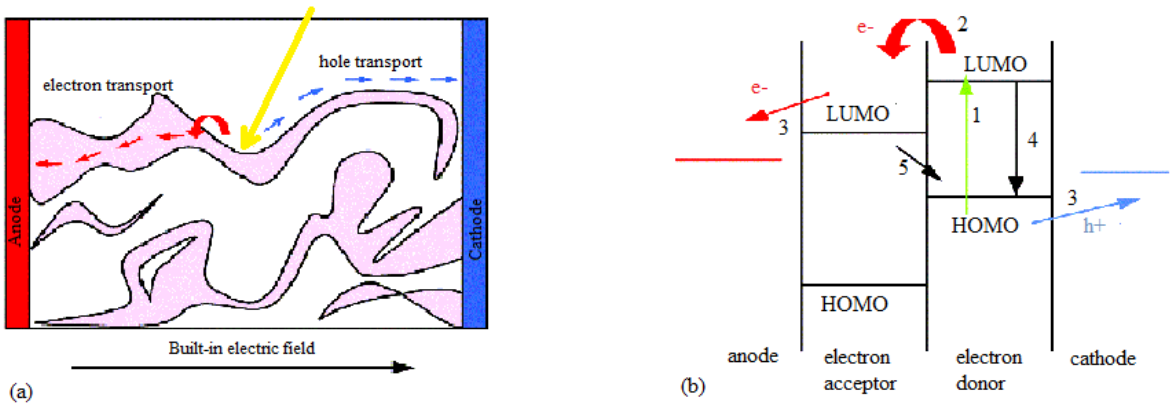

Fig. 1.12. (a) An OSC with a dispersed heterojunction, (b) a schematic of an energy-band diagram of a donor-acceptor dispersed heterojunction [adapted from 60].

Because of the large band gap in OSCs, only a small portion of the incident solar light can be absorbed. A band gap of 1.1 eV is capable of absorbing 77% of the solar irradiation on earth [70]. However, the majority of ECPs have band gaps higher than 2 eV (620 nm), which limit the harvesting of solar photons to about 30%. Conversely, because the absorption coefficients of organic materials are as high as 10^5 cm^{-1}, only 100 nm thickness of the material is necessary to absorb most of the photons (if a reflective back contact is used) [52]. *Guenes et al.* [52] therefore suggests that there is a need for a better "spectral" harvesting of solar photons through engaging lower band gap polymers and/or using energy-transfer cascades. The thicknesses of the films do not act as a bottleneck.

Additionally, for efficient dissociation of excitons, strong built-in electric fields are necessary. These can be provided by applying external electrical fields as well as via interfaces. Blending of CPs with electron acceptors, such as fullerenes, is a very efficient way to break apart photoexcited excitons into free charge carriers [52].

Current status and limitations in organic PV

Polymeric semiconductors are considered to be one of the most promising materials to lower the cost of the energy produced by SCs because they are easily processed using well-known techniques such as inkjet printing, spin casting and large scale role-to-role techniques [51]. In the last decade, important advances in bulk heterojunction SCs were achieved with the PCE exceeding 10% and reaching an estimated life time between 5-10 years. A number of strategies has been employed to achieve higher PCE: by designing and synthesizing new electron donor and electron acceptor materials with a wide photon absorption range and high mobility using adaptable third components in the active layer [71-72]; by controlling the morphology of the active layer [73]; by using buffer layers between the active layer and electrodes [74-75] and by designing and fabricating completely novel device structures [76]. As a result, OSCs currently reach PCEs of 11% [77] for single junctions and 12% [78-79] for tandem junctions with a small active area (<0.1 cm^2).

The limitation lay mainly in the stability of the SCs: the efficiency is often reduced to half in only 1.5 years [80]. The stability limitation is caused by several factors. Firstly, diffusion of metallic atoms such as In from ITO into the PEDOT:PSS (buffer layer usually) [81] and the active layer [82] as well as the PEDOT:PSS layer can also diffuse into the active layer [83]. The diffusion of metals and buffer layers reduce the stability of OSCs by changing the energy levels of buffer layers and essentially acting as traps for the charge recombination.

Secondly, metal electrodes with a low WF can be oxidized by oxygen and water permeation. The electrically insulating metal oxide layer, which is formed between the electrode and the buffer layer or the electrode and the active layer, eventually creates a transport barrier and induce an S-shaped I–V curve and thus degrade the performance of the device [84]. Oxygen penetration into the SC also activates several photo-oxidation reactions of donor and acceptor materials [85]. Changing the structures of donor and acceptor materials will alter their photon absorption, energy levels and charge carrier mobilities. In addition, the oxygen doping in the active layer can enhance hole concentration, which leads to an increase in the density of deeper traps for electrons and a decrease of the overall FF and the V_{OC} [86]. Water can diffuse into the device via e.g. the hygroscopic PEDOT:PSS and metal electrodes and it can damage the low WF metal electrodes as an oxidation agent [87]. Defects on electrodes caused by water penetration can act as pinholes to allow more water to access the device. The additional water can enter the interface of the active layer/ electrode and can form an insulating metal

oxide interlayer which decreases charge extraction [88]. In the real world, oxygen and water always simultaneously diffuse into the device and limit the stability [89].

Thirdly, after continuous long term irradiation the PCE of OSCs degrades while degradation is found to be wavelengths [90] and different light intensities [91] dependent. The fundamental reasons for the device instability are photochemical and photophysical degradation in the active layer, buffer and the active layer/electrode interface [92]. Researchers proposed some possible photo-oxidation reactions of donors and acceptors [93-94]. Photo-oxidation reactions can also occur in the buffer layer [96] and the active layer/electrode interface [97].

These reactions change the structures of donor or acceptor materials and the photoabsorption decreases, which will in its turn prevent exciton generation [97]. Additionally, these reactions lead to the formation of sub-bandgap states of materials, increasing the energetic disorder in the active layer and reducing the performance due to [3]Shockley–Reed–Hall recombination [98]. Furthermore, these reactions change the energy levels of donors and acceptors. The donor and acceptor components are not equally affected by these photo-oxidation reactions and therefore a change in the alignment of the energy levels of the donor and the acceptor (due to degradation) is observed [99]. Finally, these reactions lead to the formation of radicals on the polymeric chain, leading to so called 'relaxed' charge transfer state ($polymer^{+}/O_2^{-}$) and therefore affecting the PCE [100].

Moreover, heating is an additional factor that decreases the stability of the OSCs because structure of active layers become more unstable when the environmental temperature is higher than the glass transition temperature (Tg) of conductive polymers, e.g. in blends such as P3HT/PC61BM [101]. Finally, mechanical stress decreases the stability of OSCs . For instance, after the linear application of tension ($\varepsilon = 20\%$), devices based on P3HT/PC61BM blends, preserved only 50% of the original PCE [102-103].

[3] Shockley–Reed–Hall is a trap-assisted recombination in which the electron in transition between bands passes through a new energy state located within the band gap, created by an impurity in the structure.

Pyrrole to polypyrrole

Pyrrole (Py) has been extensively studied as it is easily oxidized, water soluble, commercially available and routes for its synthesis are well-established. Py is a heterocyclic aromatic organic compound, a five-membered ring with the formula C_4H_4NH (Fig. 1.13). It is a colourless volatile liquid that darkens readily upon exposure to air and light [104].

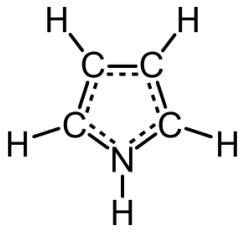

Fig. 1.13. A molecular structure of pyrrole.

Py is a precursor to polypyrrole (PPy) which offers numerous advantages including environmental stability, good redox properties and the ability to give high electrical conductivities [105-107], and has been applied in various areas [108-110].

PPy can be prepared via chemical, PEC and electrochemical polymerization [111]. The latter is usually favoured because it gives the possibility to control film thickness and morphology and results in cleaner polymers in comparison to chemical polymerization.

Electrical conductivity in the PPy film is achieved by oxidation (p-doping) or reduction (n-doping), followed by the insertion of anionic or cationic species, respectively (Fig. 1.14). The charged species which are formed upon doping are able to move along the carbon chain (delocalization) because of alternating double and single bonds in the backbone.

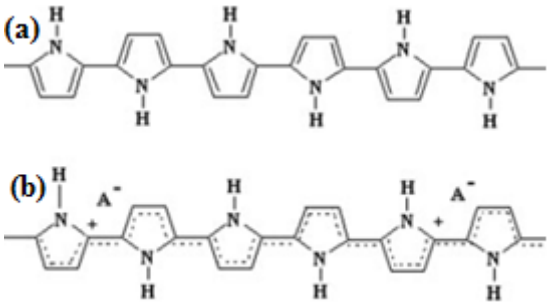

Fig. 1.14. PPy molecular structure (a) neutral and (b) doped.

Electropolymerization mechanism of Py

The electropolymerization mechanism of Py is a controversial subject and a number of mechanisms has been proposed [112-114]. The main issue lies in the determination of the different stages of polymerization process due to the speed of the polymerization. The mechanism described by *Diaz et al* [115-116] is encountered most often in the literature. *Waltman et al*.[117] and *Bargon et al*.[118] confirmed this mechanism based on theoretical studies of correlation between the reactivity and the unpaired electron density of the radical cations. In short this mechanism begins by electron transfer (E) followed by a succession of chemical reactions (C) and electron transfer reactions. The term $E(CE)_n$ which is an extension of the term ECE is often used to describe all the reactions involved in the formation of the PPy film. Detailed synthesis path can be found in different literature [119-120].

Generaly, films of PPy are electrodeposited onto a working electrode surface by anodic oxidation of the Py in an electrolytic solution. Different electrochemical methods can be used including potentiostatic (i.e. constant-potential), galvanostatic (i.e. constant current) and potentiodynamic (i.e. potential scanning i.e. cyclic voltammetry) [119]. Py dissolved in an appropriate solvent containing the desired anionic doping salt, is oxidized on the surface of an electrode by application of an anodic potential. Organic solvents such as acetonitrile (AN) or propylene carbonate are suitable due to their high relative permittivity that allows a good dissociation of the electrolyte and thus a good ionic conductivity.

Py has a relatively low oxidation potential and therefore electropolymerization can be held in aqueous solutions. As a result of the initial oxidation, the radical cation of the Py is formed and reacts with other monomers that are present in solution in order to form oligomers and finally PPy polymers. The extended conjugation in the PPy results in a lowering of the oxidation potential compared to the monomer.

Chemical polymerization of Py

Chemical polymerization of Py occurs in the presence of oxidants, such as $FeCl_3$ [121] or ammonium persulfate [122]. The mechanism of Py chemical polymerization has been studied by the kinetics of the electrochemical polymerization. The formation of the Py radical seems to be a rate determining step. Likewise, *Tan et al*.[123] showed that the mechanism of Py polymerization by chemical oxidation is similar to that by electrochemical polymerization, by studying kinetics of the reaction in aqueous solution. The possible mechanism is shown in

Fig. 1.15, and is consistent with a study of *Ayad et al*. [121] who showed that the interaction occurs between a radical cation and monomer or oligomer chain.

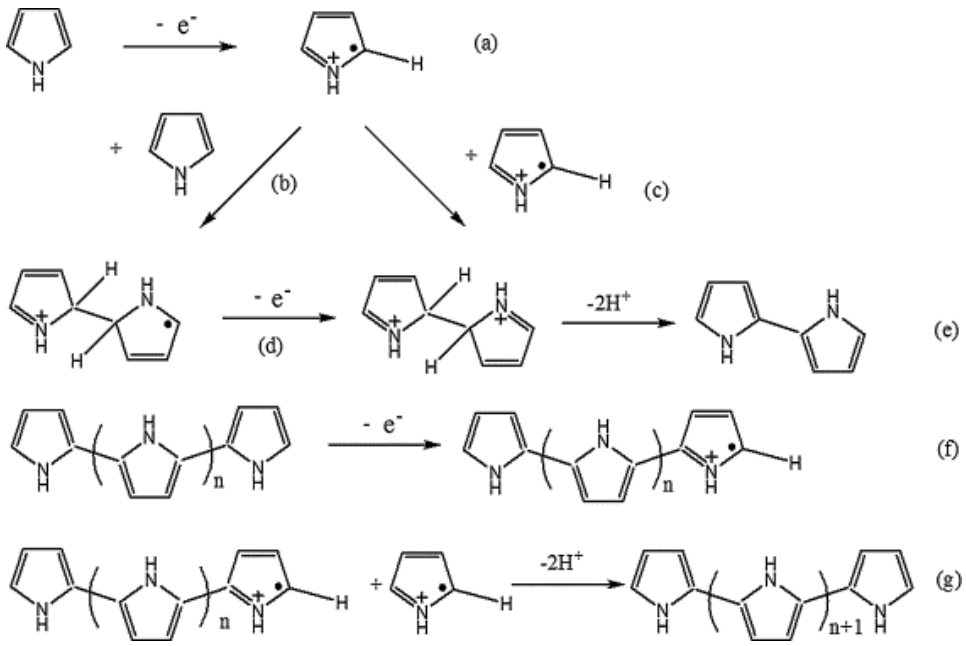

Fig. 1.15. Chemical polymerization of Py: the mechanism [adapted from 123].

The resulting polymer in its oxidized form is conducting with charge compensation given by $FeCl_4^-$. The conductivity of PPy film induced from the presence of different ferric salts (i.e. effect of dopant ion) has been related to the Fe^{2+}/Fe^{3+} redox potential with strong acid anions providing the most oxidizing ferric species. Weaker acid anions typically coordinate Fe^{3+} ions more strongly, reducing its oxidizing potential [124]. The conductivity of PPy increases as the synthesis temperature is reduced due to reduced number of side reactions [125].

The individual polymerization methods are simultaneously used as deposition methods of PPy onto different substrates. Electrochemical and PEC deposition of PPy onto different substrates can be considered as the electrochemical deposition while chemical polymerization is used in cases where PPy is deposited onto substrates by spin casting.

1.3. Photoelectrochemical Polymerization of Py

This method utilizes photogenerated holes in the V_B of semiconductors to polymerize the monomers. It is a selective deposition of polymers on different photoactive substrates. The ED is performed under illumination, to exploit the intrinsic semiconductor behaviour of the working electrode [126]. Illumination has at least two beneficial effects: (a) it increases conductivity (photoconductivity), (b) it directly initiates polymerization at the irradiated SC surface by using the photogenerated holes to oxidize the monomer molecules. Additionally, reduced applied potentials are used with the assistance of light.

Upon oxidation of the Py monomers radical cations are formed. These radical cations initiate the polymerization procedure, which eventually leads to the formation of an oligomeric or polymeric film on the surface of the working electrode [127]. Formation of such film, however, impedes further exciton generation and charge separation (and consequently PEC polymerization) due to optical and electrical shadowing, respectively [126].

PEC polymerization of Py has not been extensively studied although the combination of this method with regards to Py was expected to become a key technology in the fabrication of organic devices [128].

Mechanism of PEC Polymerization

In case of inorganic materials having low conductivity, high potentials must be applied resulting in polymer overoxidation. Light causes the conductivity of the semiconductor to increase (photoconductivity). PEC polymerization (deposition) occurs at the irradiated semiconductor surface/electrolyte interface. Upon irradiation, electrons from the VB are promoted to the CB. Subsequently, these electrons are extracted into external circuit by applying external bias potential while the photogenerated holes react with species in the solution such as solvent, electrolyte anions or monomer. The polymerization starts upon monomer oxidation. Subsequently the radical cation reacts with another radical cation or alternatively with a monomer to form dimer. Again, dimer can react further with either a monomer or oligomer radical cation and as a result, polymer is formed. This method employs the band edge positions of the semiconductor as well as the oxidation potential of the species in the solution. The mechanism is shown in Fig. 1.16 [129].

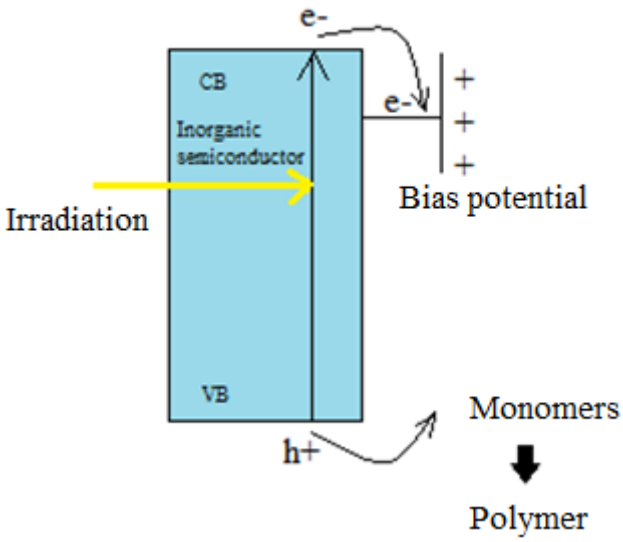

Fig. 1.16. Schematic illustration of a PEC polymerization of a monomer on an inorganic semiconductor electrode.

The values of the applied potential are not high enough to electrochemically oxidize the monomer. The role of the applied potential in this case is to supress the recombination of the photogenerated charge carriers [129].

Some inorganic semiconductors are susceptible to photocorrosion under anodic conditions which leads to degradation of the electrode as well as lowering the efficiency of the polymerization process. This happens because only a small fraction of photogenerated holes can oxidize the monomer in photocorroded environment [129].

In comparison with electrochemically prepared polymers, PEC polymerization is less dependent on the nature of the electrolyte with respect to the morphology and the conductivity of the final polymer films [130]. This is assumed to be a result of considerably slower polymerization process in comparison with that of electrochemical polymerization.

The growth of the polymer is eventually terminated by both electrical and optical shielding of the deposited active area of the inorganic semiconductor. This method has been successful in preparation of various SC structures: deposition of ECPs on CdS, CdTe [131], $CdSe_xZnS$ [132], nanostructured materials such as nanoporous WO_3 and TiO_2 [126-127] as well as other ECPs such as PEDOT [133].

Nucleation Process and Formation of Thin Film

Nucleation and film growth is a complex mechanism, made up of different steps. Different processes can be involved in the nucleation growth mechanism (NGM) and, often, they can occur either simultaneously or successively. The (NGM) of conducting polymers requires the oxidation of monomers which are either adsorbed on the electrode surface or come from the solution. The oxidized monomers diffuse towards the interface where oligomerization happens and oligomeric high density region (OHDR) is formed. The polymer nucleation process and subsequent growth of thin film at the electrode surface depends on the degree of saturation of the high density oligomers (i.e. on OHDR). In other words NGM is given by the solubility of the oligomers present at the electrode/solution interface. When growing oligomer at the interface reaches a critical chain length, which makes it insoluble in the electrolytic solution, supersaturation is reached, clusters are deposited onto the electrode, and nuclei growth begins [134-135].

Romero et al. [136] showed that the higher the temperature the lower the polymerization onset potential. This implies that at lower temperature more energy is required to achieve oxidation of monomer, and this in turn requires application of higher oxidation potential. Another finding by *Romero et al*. was that the induction time increases with temperature decrease. Induction time is the time required to exceed oligomers saturation level at the electrode-solution interface.

Polymers synthesized at low temperatures (~ 268 K) show a slightly lower conductivity than those synthesized at the higher temperatures (~ 303 K). As temperature also affects monomer solubility and it has a profound effect on the reaction kinetics, it therefore has an effect on oligomer formation rate [136-137].

A NGM by OHDR in the electrode–solution interface, formed by oligomers with different chain lengths, has been confirmed by different studies. It has also been confirmed that, depending on different conditions (e.g. applied potential, electrolysis time, concentration, etc) it is possible to control to some extent the oligomer to be generated [138-139].

To conclude current-time transients revealed that a temperature decrease caused an induction time increase, suggesting that at these low temperatures the process is much slower and takes longer to precipitate the oligomers that produce the first nuclei growth. The conductivity of the ECP film is also affected by the deposition temperature, showing lower conductivities for films deposited at lower temperatures.

1.4. Hybrid SCs

Organic-inorganic junctions have created a great deal of interest for their potential in developing hybrid SCs. Organic/inorganic hybrid SCs combine organic and inorganic semiconductor material, with the intention to combine the advantages of both material groups [140]. Usually, the inorganic electron acceptor material provides further advantages to the system, while maintaining low cost processability. Inorganic acceptor materials are more environmentally stable than organic materials [141].

Firstly, combining inorganic semiconductor materials with ECPs could provide a solution to the photo-induced degradation of the conjugated organic semiconductors [142]. Secondly, photogeneration of charge carriers can be achieved by excitons absorbed in the inorganic material [143]. The contribution of light absorption by an inorganic acceptor has the potential to be greater than the absorption contribution of ECPs in OSC [144]. Additionally, the combination of such materials provides the possibility to create a complementary absorption profile [145]. Thirdly, the physical dimensions of some inorganic semiconductors can be synthesized into vertically well-aligned nanostructures [146]. This allows device architectures with efficient exciton dissociation and electron transporting route.

Device structure

The structure and operating principle of hybrid SC is similar to that of OSC, the only difference being that the organic electron accepting material is replaced by an inorganic semiconducting material. The majority of hybrid SCs are planar in nature: blends and bilayers, composed of a photoactive layer wedged between two electrodes of different work functions. The device itself is deposited on a transparent substrate, usually TCO/glass or flexible PET substrates [142].

The anode consists of a semi-transparent oxide layer ITO. Its role is to allow light to pass through, and to collect holes from the device. A conductive polymer blend is applied between the anode and the photoactive layer. This thin layer is mostly spin coated on top of the TCO surface. The polymer blend layer serves several functions. As well as a hole transporting layer and exciton blocker, it smoothes the TCO surface, encapsulate the active layer from oxygen, and stops the cathode material from diffusing into the active layer, which can lead to unwanted trap sites [147]. The absorber photoactive layer containing a donor and acceptor material is sandwiched between two electrodes (Fig. 1.17) The cathode is usually aluminium, but calcium or magnesium is sometimes used. The function of the cathode is to collect electrons from the device.

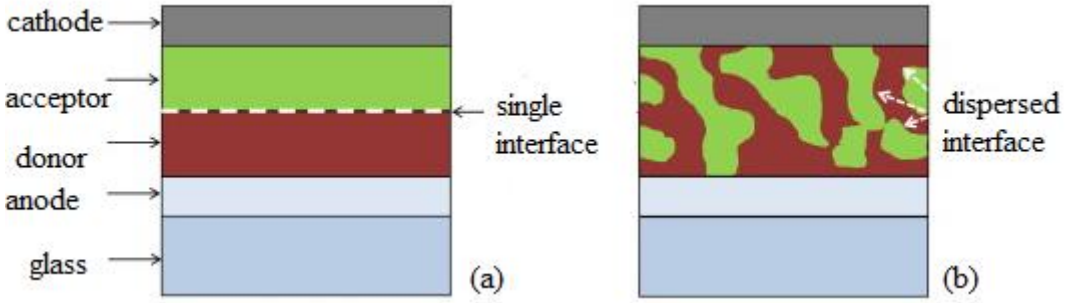

Fig. 1.17. A schematic of a general hybrid SC structure with (a) bi-layer structure and (b) bulk heterojunction (blend) structure [adapted from 12].

Device operation

Upon irradiation of the photoactive layer, an excited state is formed; however, the electron and hole are coulombically bound as opposed to inorganic semiconductors in which incident photon breaks a covalent bond, which forms an exciton. Exciton can be dissociated at a D/A interface. When separated, the electron travels to the acceptor material at the interface and is transported to the cathode for charge collection. The hole produced in the donor material travels through the polymer and is collected at the anode [12]. This process is displayed as in Fig.1.18.

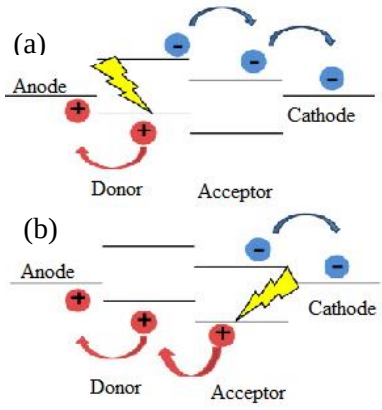

Fig. 1.18. Schematic diagram displaying charge transfer for (a) photo-generation in the electron donor, and (b) photo-generation in the electron acceptor.

The inorganic acceptor material may also contribute useful photocurrent. When light strikes and is absorbed in the acceptor material, an exciton is formed which must be dissociated by the offset in energy of the donor HOMO level and the acceptor valence band edge (Fig.1.19).

The hole travels to the donor at an interface and is transported to the anode while the electron remains in the acceptor material and travels to the cathode for collection (Fig. 1.18 (b)).

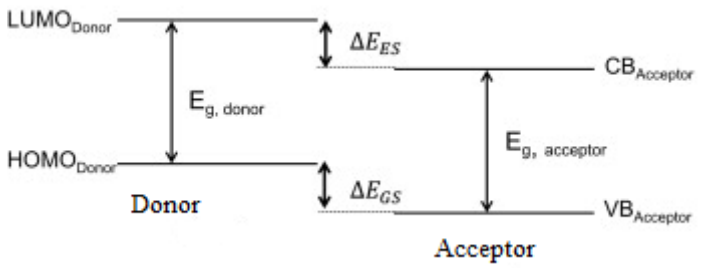

Fig. 1.19. General energy band diagram of the heterojunction formed in a hybrid SC.

The choice of materials used in hybrid SCs is crucial to the overall efficiency. The donor material, must have both electronic composition and good hole mobility properties. Particularly important are the band gap and the HOMO and LUMO levels, with respect to the acceptor material. Since the discovery of ECPs poly (3-hexylthiophene) (P3HT) became the favoured polymer donor material. Regio-regular P3HT has many advantages when compared to e.g. poly(p-phenylene vinylene)(PPV), such as a higher hole mobility, improved absorption and good environmental stability [148].

Further, the blend of P3HT:PCBM has been researched extensively, and large optimisation was achieved for parameters such as solvent used [149-150]. Chemical structures for some of the polymer materials used in OPV and hybrid devices are displayed in Fig.1.20.

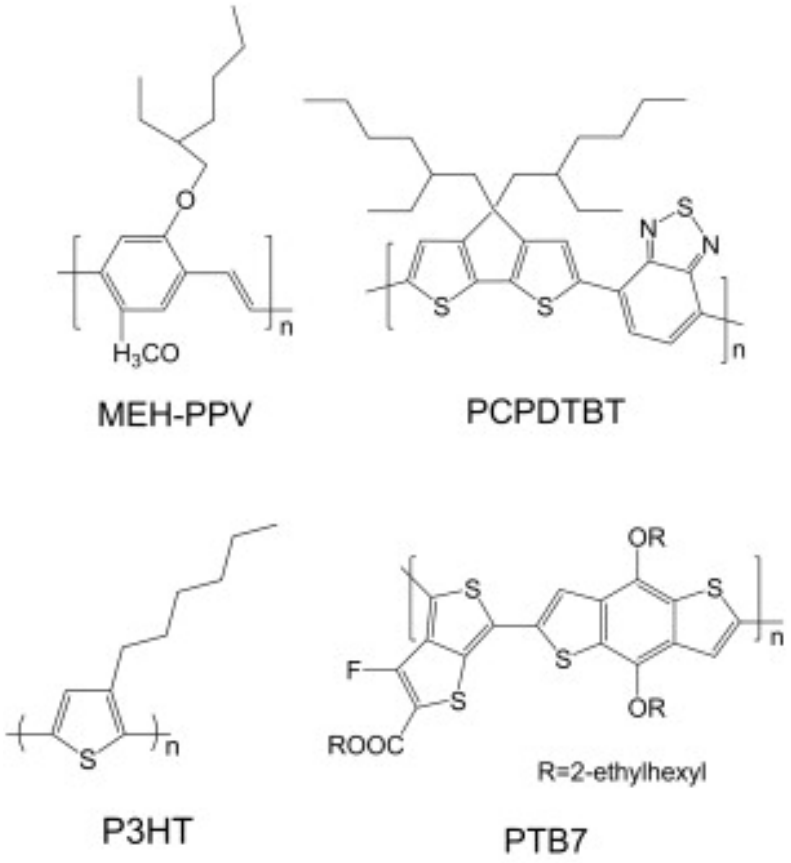

Fig. 1.20. Some of the ECPs used in OSCs and hybrid structures.

In recent times, poly({4,8-bis[(2-ethylhexyl)oxy]benzo[1,2-b:4,5-b′]dithiophene-2,6-diyl}{3-fluoro-2-[(2-ethylhexyl)carbonyl]thieno[3,4-b]thiophenediyl})(PTB7) has been studied and displayed great photovoltaic performance [151]. This polymer has a band gap of ~1.6 eV, and displays good hole mobility, good solubility in organic solvents and polymer alignment which helps with charge transport [152].

When it comes to acceptor material, fullerenes have certain advantageous traits when combined with P3HT, such as excellent solubility, but they also show limitations such as restricted environmental stability and absorption contribution [153]. Using an inorganic material instead of fullerene can help to overcome some of these limitations. One of the main advantages of inorganic semiconductor nanoparticles is the tunability of their band gap, which results from the modifications of the nanoparticle [154].

A number of materials has been investigated as an electron acceptor in hybrid SCs. These include CdSe [155], CdS [156], CdTe [157], c-Si [158], PbS [159], TiO_2[160], ZnO [161],

ZnS [162]. These materials all have adequate electronic characteristics which can be used in design of hybrid SCs.

As literature review shows, PPy as a ECP used in hybrid SCs has not been researched extensively. In addition, there is a limited number of studies focused on hybrid SCs based on PPy using electrochemical polymerization [131- 163]. Examples of a studies focusing on this topic include *Inganas et al.* [23] and *Yoneyama et al.* [164] who studied PEC deposition of PPy onto a-Si:H yet exluded PCE of the devices.

.

1.5. Scope of the Present Work

Based on the literature review it is clear that both, a-Si:H and ECPs have several advantages which could bring potential benefits to PV industry. Most important, perhaps, is their high absorption coefficient value which enables production of light thin film SCs. a-Si is suitable due to its abundance, the low production cost in comparison with c-Si, it is a non-toxic material that can be produced as thin films reducing the bulkiness of SCs. ECPs showed to be a promising material in the PV industry. They are easily processible by different methods, have high conductivity when doped and their conductivity is tunable. ECPs can be deposited using several methods yet the PEC polymerization has not been extensively used with respect to production of hybrid SCs.

The current work focuses on preparation of hybrid SC with a PPy/i-a-Si:H/n-a-Si:H/AZO/glass n-i-p structure, in which PPy is deposited using PEC deposition method. The focus is to study a novel selective deposition method while employing the benefits of both PPy and a-Si:H materials.

1.6. The Aim of the Study

The aim of this research is to develop hybrid SC based on a-Si:H, with PPy functional layer fabricated at room temperature, using photo-assisted ED at low applied potentials and short deposition times. In our study the conventional p-type a-Si layer used for n-i-p a-Si based “superstrate” SCs has been replaced by a PPy film to prepare PPy/i-a-Si:H/n-a-Si:H/AZO/glass hybrid SCs.

In this thesis, deposition of the PPy film was studied by cyclic voltammetry (CV) and linear sweep amperometry. The main novelty of this study is the possibility to deposit PPy onto a-Si:H at a reduced potential and therefore avoid overoxidation of the PPy film as well as to achieve uniform selective deposition onto the photoactive a-Si:H electrode surface.

Therefore, to sum up the present investigation is aimed at following objectives:

- To synthesize PPy thin films by PEC deposition method under different applied potentials, light sources and employing different dopant salts.
- To characterize morphological, optical and electrical properties of obtained PPy films and complete hybrid structures.

Chapter II: Experimental Details

Hybrid p-PPy/i-a-Si:H/n-a-Si:H/AZO/glass PV structures were obtained on the i-a-Si:H/n-a-Si:H/AZO/glass substrates which were prepared using PECVD technique by the NEXT ENERGY Company (Germany) [165]. Prior to the solution making, Py (Sigma Aldrich) was distilled under vacuum, at temperature just below 60 °C and collecting flask with Py was covered with aluminium foil to prevent oxidation by light (Fig. 2.1).

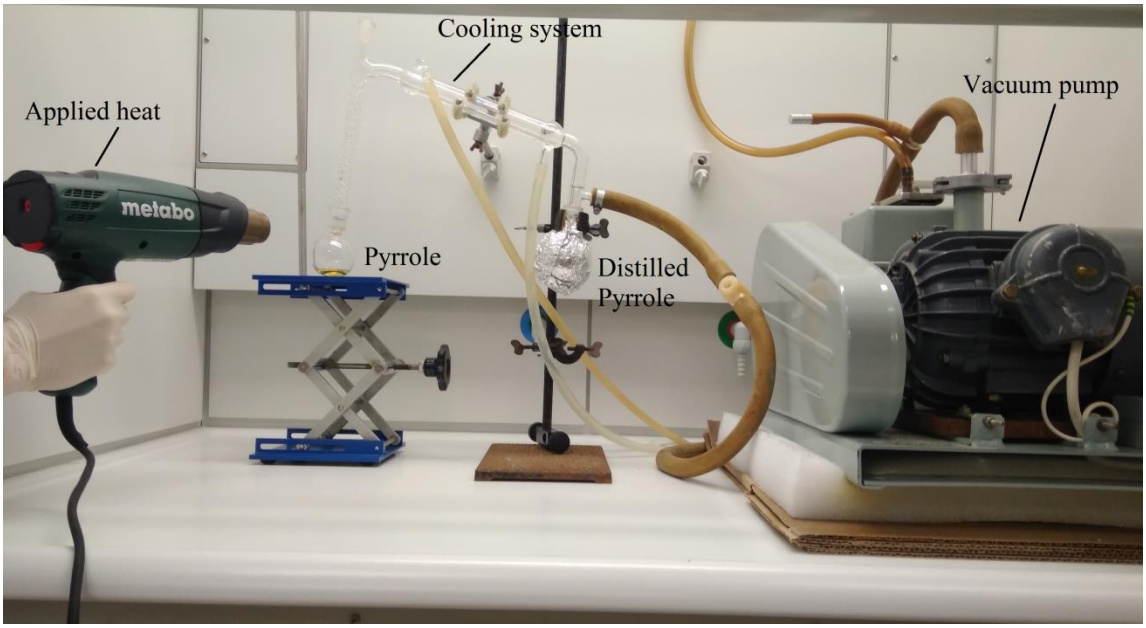

Fig. 2.1. An experimental set-up for Py distillation.

An aqueous solution containing 0.3 M Py and 0.1 M naphtalene-1-sulfonic-acid sodium salt (NSANa) dopant (Fig. 2.2) was prepared.

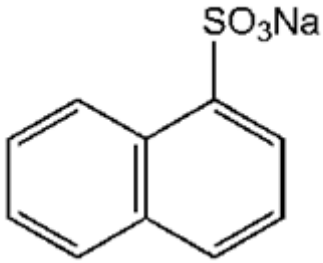

Fig. 2.2. The molecular structure of the NSANa dopant.

Cyclic voltammetry

In order to find optimal parameters for PPy thin film ED, the i-a-Si:H/n-a-Si:H/AZO/glass electrodes were examined by CV in the three-electrode cell in a working solution containing 0.3 M Py and 0.1 M NSANa. CV was performed in the potential range from -0.1 V to 1.0 V vs. SCE in dark and under Xe lamp and red laser light illumination of 100 mW/cm^2 and 5 mW/cm^2 intensity, respectively.

An experimental set up consists of a standard three-electrode electrochemical cell and a potentiostat/galvanostat Autolab PGSTAT 30 controlled by a PC. The electrochemical cell consists of a vessel with working electrode (WE), counter electrode (CE), reference electrode (RE) immersed into the working electrolyte solution. In our case, the WE was i-a-Si:H/n-a-Si:H/AZO/glass substrate, the CE was a Pt plate, and the RE was saturated calomel electrode (SCE).

In general, the WE's potential is varied linearly with time, while the RE maintains a constant potential. The CE provides current flow from the source to the WE. The electrolyte solution provides ions to the electrodes during oxidation and reduction processes. A potentiostat/galvanostat is an electronic device which uses a direct current (DC) power source to produce a potential or current which is maintained and accurately determined. The current-to-voltage converter is responsible for measuring the resulting current and the data system produces the resulting voltammogram (Fig. 2.3) [166].

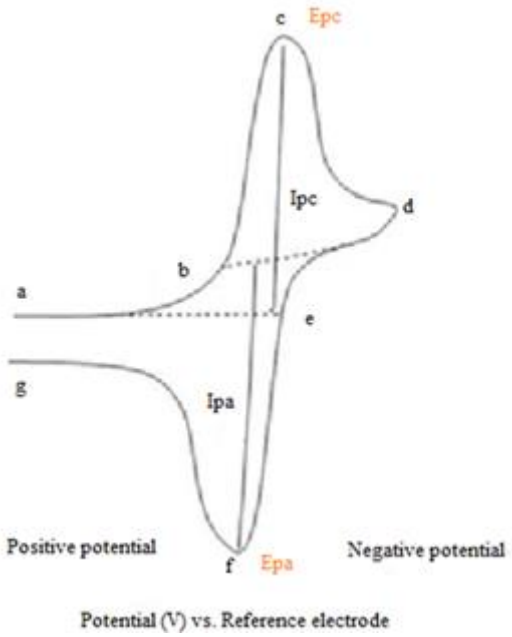

Fig. 2.3. A schematic cyclic voltammogram.

The reduction process occurs from the initial potential (a) to the switching potential (d). The switching potential is the point where the voltage is sufficient enough to cause reduction or oxidation of the analyte.

Generally, potential is first scanned negatively to cause reduction. The resulting current is called cathodic current (I_{pc}). The corresponding peak potential occurs at (c), and is called the cathodic peak potential (E_{pc}). The E_{pc} is reached when all of the substrate at the surface of the electrode has been reduced. After the switching potential has been reached (d), the potential scans positively from (d) to (g). This results in anodic current (I_{pa}) and oxidation occurs. The peak potential at (f) is called the anodic peak potential (E_p), and is reached when all of the substrate at the surface of the electrode has been oxidized [166].

CV can be used to study qualitative information about electrochemical processes such as the presence of intermediates in oxidation-reduction reactions or the reversibility of a reaction. Additionally, CV can be used to determine the system's electron stoichiometry, concentration of an unknown solution, analyte's diffusion coefficient and the reduction/oxidation potential, which can be used as an identification tool.

Photoelectrochemical deposition

Conducting polymer functional layers of PPy doped with 1-naphtalene sulfonate (NSANa) and p-TSA were deposited potentiostatically (Autolab PGSTAT-30 potentiostat/galvanostat) in a standard electrochemical cell onto the photo-active i-a-Si:H/n-a-Si:H/AZO/glass WE with Pt CE and SCE RE. The electrochemical polymerization was performed at a room temperature (21 °C) by the assistance of red laser light illumination (670 nm, 5 mW/cm^2) (Fig. 2.4 (a))and Xe lamp (100 mW/cm^2).(Fig. 2.4 (b)). The samples were illuminated from the glass side in order to provide continuous polymerization on the surface of the a-Si photoabsorber. The applied potentials were in the range from 0.2 V to 0.5 V vs. SCE and the polymerization time varied from 20 s to 50 s (series 1) and 220 to 330 s (series 2) (Fig. 2.4). The temperature of the solution was continuously measured during the deposition time and no temperature rise was detected. The general idea of the PEC deposition is described in the literature review.

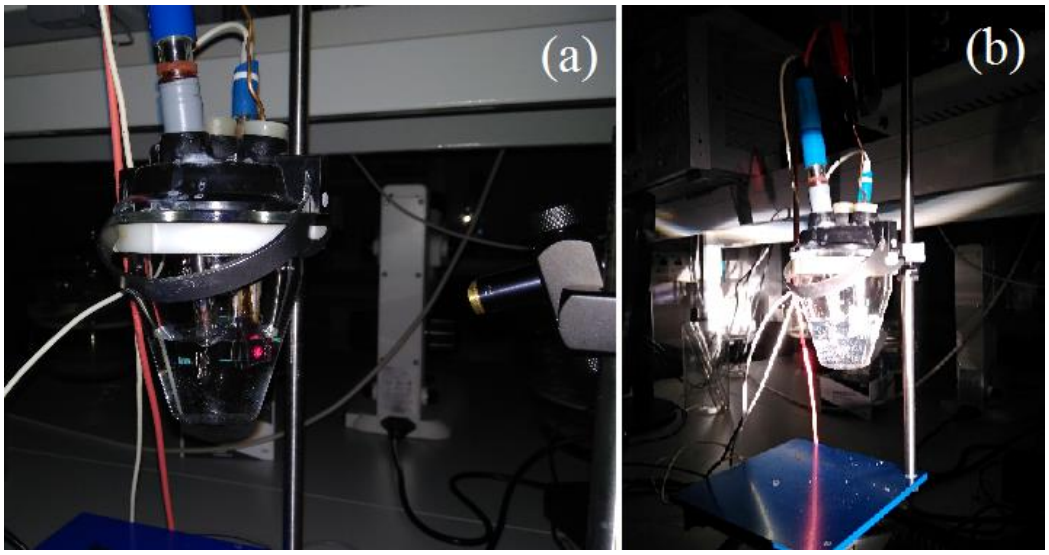

Fig. 2.4. The set up for PEC deposition using (a) laser beam and (b) Xe lamp irradiation.

Post-treatment and back contacts

The structures were immediately dried after PEC deposition under the nitrogen gas flow. In order to eliminate excess moisture in the structures, the prepared hybrid structures were left in an oven for 15 min at 60 °C. Subsequently, two different types of back contacts were applied to the polymer film. Au back contacts with a thickness of ~20 nm were applied by high vacuum evaporation (HVE) (BOC-EDWARDS Auto 500 evaporation system). Alternatively, highly conductive water based graphite suspension (Alfa Aesar) contacts were painted onto the PPy layer and dried in an oven at 60 °C for 15 min.

Characterization methods

Photoelectrochemical performance

The PEC characterization of the structures was performed in the range from 1 V to -1.3 V vs. SCE in a 0.1 M Na_2SO_4 background solution under chopped white light with the intensity of 100 mW/cm^2. The i-a-Si:H/n-a-Si:H/AZO/glass electrodes with and without PPy top layer were examined.

The PEC measurements (i.e. transient photocurrent (TPC)) allow to study the extraction of minority charge carriers generated by the light absorption in semiconductors. PEC performance can be studied only in corrosive media as minority holes or electrons take part in the anodic or cathodic reactions on the electrode-electrolyte interface, respectively [167]. When the device is excited with pulses of light, the photogenerated charges are extracted on

the electrodes, resulting in the increasing current, which is detected by the potentiostat. There are two ways to measure TPC: in the “light on” and the “light off” positions (Fig. 2.5).

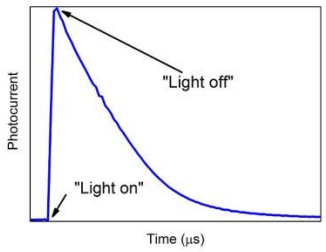

Fig. 2.5. TPC plot.

In the “light on” position the signal is recorded as soon as the excitation pulse is switched on, allowing to measure the build-up of charges on the electrode after the start of excitation. The “light off” measurement shows how the charges decay after the pulse is switched off. In contrast to the transient photovoltage, TPC measurements are conducted under short circuit condition and provide information about charges, charge recombination and density of states. Additionally, TPC measurements help to construct “drift-diffusion” model which reflects trapping and de-trapping of the photogenerated charges and the quality of contact between different layers [168-169]. Furthermore, TPC allows varying different measurement parameters, such as intensity or length of the light pulse, applied voltage, photosensitivity of the device etc.

HR-SEM

The thickness of polymer films as well as morphology were analysed by high-resolution scanning electron microscopy (HR-SEM, Zeiss Merlin) equipped with an In-Lens SE detector for topographic imaging and In-Lens energy selective backscattered detector for compositional contrast.

HR-SEM scans a sample with a focused electron beam where the electrons interact with atoms in the sample, producing various signals that contain information about the sample's surface topography and composition (Fig. 2.6).

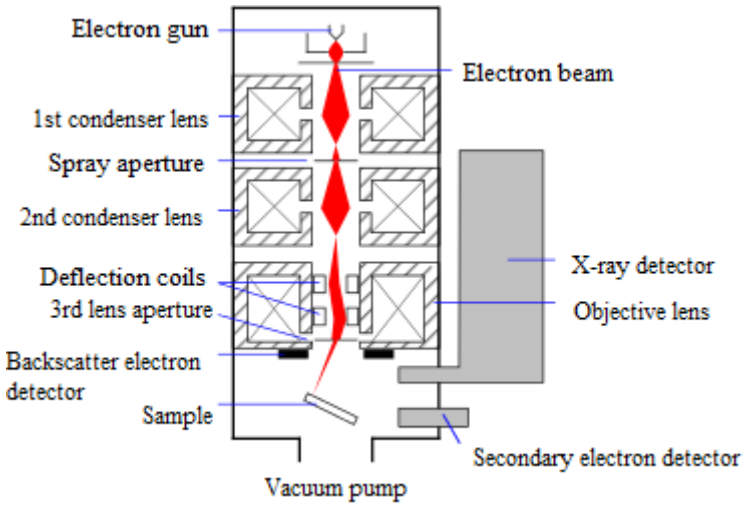

Fig. 2.6. A schematic of an SEM (adapted from 169).

Samples can be observed in low and high vacuum, in low vacuum, in wet conditions, and at a wide range of cryogenic or elevated temperatures. The most common SEM mode is detection of secondary electrons emitted by atoms excited by the electron beam. The number of secondary electrons that can be detected depends, among other things, on the sample's topography. By scanning the sample and collecting the emitted secondary electrons using a special detector, an image displaying the topography of the surface is created [170].

Ultraviolet–visible spectrophotometry

The optical measurements were recorded using Agilent Cary5000 UV-VIS-NIR spectrophotometer as a function of wavelength in the range of 300-1500 nm to determine the optical absorption coefficient and energy band gap.

The optical band gap was estimated from Tauc's equation [171]:

$$(\alpha h\nu) = A(h\nu - E_G)^n \qquad (2.1.)$$

where A is a constant, E_G is the energy gap and n=0.5 for allowed direct transition and n=2 for allowed indirect transition. In the case of direct transition, $(\alpha h\nu)^2$ versus $h\nu$ graph will have a linear region, extrapolation of which to $\alpha h\nu=0$ will show the direct band gap. Similarly, indirect band gap can be obtained from $(\alpha h\nu)^{1/2}$ versus $h\nu$ graph.

Ultraviolet–visible spectrophotometry (UV-Vis) refers to absorbance/transmittance spectrophotometry or reflectance spectrophotometry in the ultraviolet-visible spectral region (Fig.2.7). This means it uses light in the visible and adjacent (near-UV and near-infrared) ranges.

UV-Vis spectrophotometery is based on the principle of electronic transition in atoms or molecules upon absorbing allowed energy from an incident light that allows electrons to be excited from a lower energy state to a higher excited energy state. While interaction with infrared light causes molecules to undergo vibrational transitions, the shorter wavelength with higher energy radiations in the UV (200-400 nm) and visible (400-700 nm) range of the electromagnetic spectrum causes many atoms/molecules to undergo electronic transitions [172].

The optical E_G, expressed in eV, depends on the incident photon wavelength by means of a Planck relation:

$$E_G = h\nu = h\,\frac{c}{\lambda} \qquad (2.2)$$

where h = the Planck constant ($6.62 \cdot 10^{-34}$ J s); ν = the wave frequency and c = light speed in vacuum ($3 \cdot 10^{8}$ m/s). Experimentally, the E_{opt} of the thin film is estimated by linear extrapolation from the absorption feature edge to energy axis (A= 0).

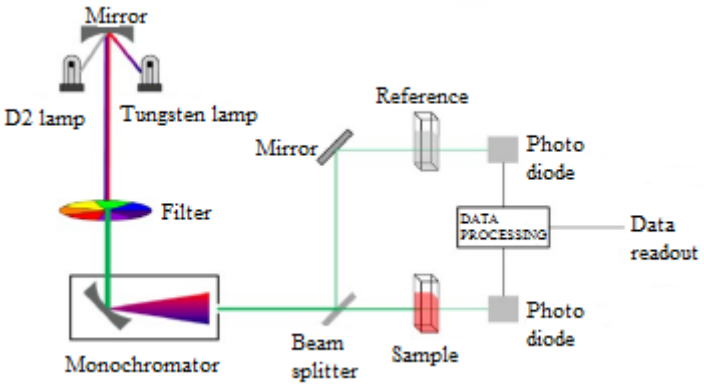

Fig. 2.7. A schematic of the UV-Vis spectrophotometer.

Since the absorption spectrum reveal information on electronic transition, the onset of absorption is considered as the E_G of semiconductor or ECPs. In some case, the peak of the absorption spectrum is also considered as the E_G. Fig. 2.8 gives an example of the E_G approximation for an ECP (denoted as Polymer-X) in solution and film.

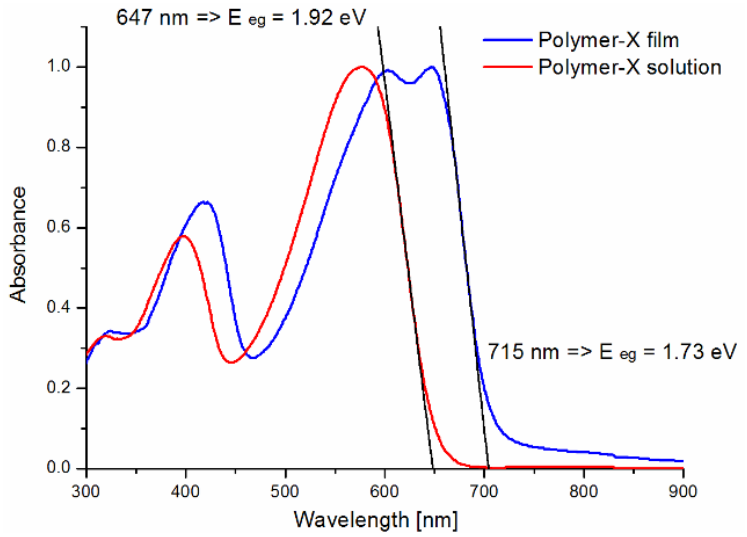

Fig. 2.8. Determination of the E_G from a UV-Vis spectra.

Generally, the color of a molecule in the solution or the film gives an indication of their E_G. The color of a film or solution that an observer perceives is usually the complementary wavelength of the electromagnetic spectrum that the molecule absorbs. For example, if a molecule in solution or film appears green in color, then the molecule is absorbing (and therefore has an E_g) complementary color to green, which is red [173].

Kelvin probe measurements

Surface potential (SP) changes for the prepared a-Si structures without and with the electrodeposited PPy layer were measured by the ambient scanning Kelvin probe system (SKP5050) equipped with a 2 mm gold-covered vibrating tip and under pulsed red laser beam illumination (670 nm, 5 mW/cm^2 intensity).

The Kelvin probe is a non-contact, non-destructive measurement device used to investigate electrical properties of materials. It is based on a vibrating capacitor which measures the WF difference between a conducting specimen and a vibrating tip or, for non-metals, the SP which is a difference between WF of the tip and a particular material (Fig. 2.9.) [174]. The WF is the minimum thermodynamic work (i.e. energy) needed to remove an electron from a solid to a point in the vacuum immediately outside the solid surface . The WF is an extremely sensitive indicator of surface condition and is affected by adsorbed or evaporated layers, surface reconstruction, surface charging, imperfections, surface and bulk contamination, etc. [176].

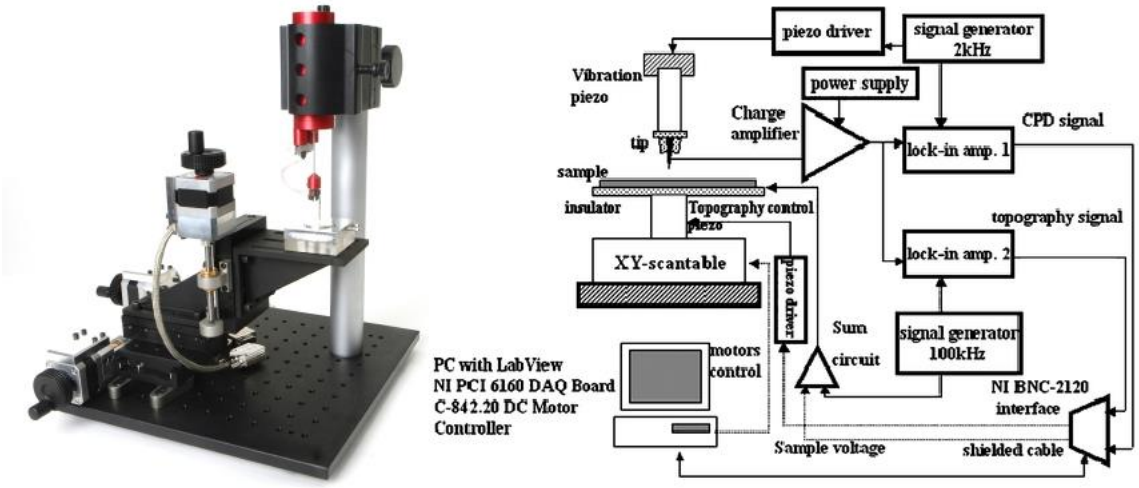

Fig. 2.9. A general Kelvin probe schematic set-up (adapted from 175).

Current density –Voltage (J-V) characteristization

J-V characteristics were measured using the Autolab PGSTAT-30 potentiostat/galvanostat. J-V characterization of the obtained SC was held under a calibrated halogen lamp with an illumination intensity of 100 mW/cm^2. The samples were illuminated from the glass side.

The J-V curve of a SC is the superposition of the J-V curve of the SC diode in the dark with the light-generated current (Fig. 2.10).

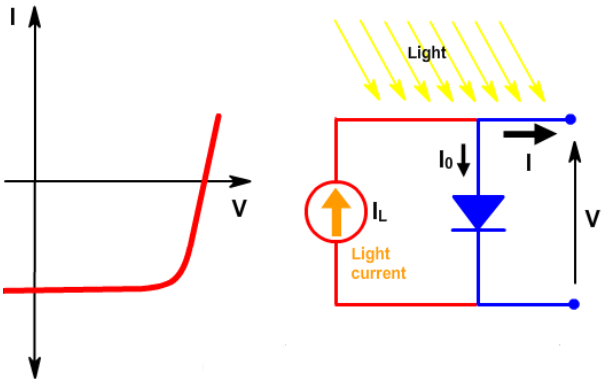

Fig. 2.10. The effect of light on the current-voltage characteristics of a p-n-junction. The greater the light intensity, the greater the amount of shift (adapted from 177).

The light has the effect of shifting the J-V curve down into the fourth quadrant where power is extracted from the diode. Illuminating a cell adds to the normal dark currents in the diode so that the diode law becomes:

$$I = I_0 \left[\exp\left(\frac{qV}{nkT}\right) - 1\right] - I_L \quad (2.3.)$$

where I = the net current flowing through the diode; I_0 = "dark saturation current" (the diode leakage current density in the absence of light); V = applied voltage across the terminals of the diode; q = absolute value of electron charge; k = Boltzmann's constant; T = absolute temperature (K); and I_L = light generated current.

The short-circuit current (I_{SC}), the open-circuit voltage (V_{OC}), the fill factor (FF) and the efficiency (η) are all the parameters determined from the J-V cuerve.

The I_{SC} is the current through the SC when the voltage across the SC is zero (i.e., when the SC is short circuited) whereas the V_{OC} is the maximum voltage available from a SC, at zero current. The I_{SC} and the V_{OC} are the maximum current and voltage respectively from a SC. However, at both of these operating points, the power from the SC is zero. The FF is a parameter which, in conjunction with V_{OC} and I_{SC}, determines the maximum power (P_{MAX}) of a SC. The FF is defined as the ratio of the P_{MAX} from the SC to the product of V_{OC} and I_{SC}. The PCE η is defined as the ratio of energy output from the SC to input energy from the sun. In addition to reflecting the performance of the SC itself, the efficiency depends on the spectrum, intensity of the incident sunlight and the temperature of the SC [177].

Chapter III: Results and Discussion

Cyclic voltammetry

The i-a-Si:H/n-a-Si:H/AZO/glass electrodes were analyzed by the CV in order to determine appropriate potential values for the PPy electrodeposition. The CV shows the significant influence of the illumination on the electrochemical system equal to the electrodeposition system (Fig. 3.1). A well-defined anodic peak at around 0.2 V appears under the Xe lamp illumination. All the anodic peaks shown in Fig. 3.1 correspond to the oxidation of Py and formation of a PPy layer doped with NSA on the surface of i-a-Si [178-179]. The advantage of using the laser beam spot illumination is the possibility to deposit the polymer only on a restricted photo-activated area. Using the Xe lamp leads to a full coverage of the i-a-Si:H anode surface immersed into the working solution. In the dark oxidation peak of Py to PPy has onset potential at about 0.65 V. As noted, at values higher than 1 V a decrease in Py activity occurs and the polymerization process rate decreases due to overoxidation of the PPy layer [180-182]. In an aqueous solution under anodic potentials at which overoxidation occurs PPy is irreversibly oxidized leading gradually to a non-conducting material formation; PPy is de-doped as the dopant anions are removed from the polymer matrix [183].

Intensive illumination helps to improve dramatically the rate of the PPy formation and also allows to lower the deposition potential value. The onset potential for illuminated structures appears in the negative region. The main roles of illumination during the polymerization process are: it affects the initial stages of polymerization by creating the additional oxidative potential on the i-a-Si:H surface and it enhances the nucleation process of Py on i-a-Si [184]. It can be noted that in the case of laser illumination anodic current density on the reverse sweep is higher than on the forward sweep, creating a crossover point. The crossover of the anodic part of the CV is typical for surface phase formed by a nucleation and growth [185]. The observation of a crossing point in the CV is unusual; for an oxidation process; it signifies the formation of a product that has a much lower reduction potential. In our case the higher anodic current on the reversed sweep suggest that the potential required for the PPy deposition on the PPy film (formed during the forward scan) is lower than that required for the PPy deposition on the Si surface, i.e. Py oxidizes more readily on PPy than on the i-a-Si:H surface [186]. Additionally, the increase of the current at a potential around 0.6 V corresponds

to intensified anodic reactions running of the n-i a-Si:H electrode surface with participation of photo-injected minority holes (see also Fig. 3.5).

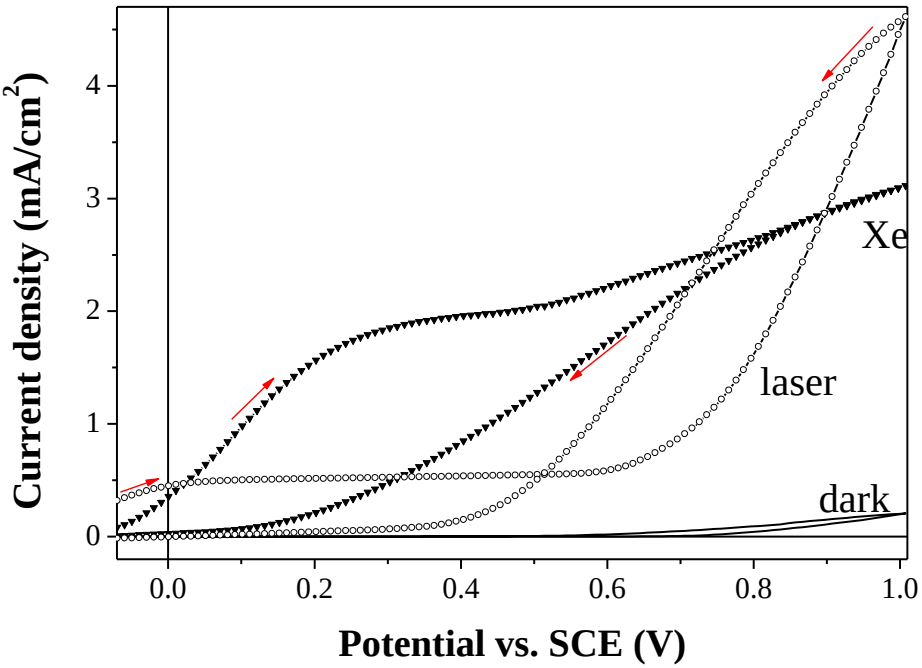

Fig. 3.1. CV on i-a-Si:H/n-a-Si:H/AZO/glass electrode in 0.3 M Py/0.1 M NSANa aqueous solution measured at a scan rate of 20 mV/s in dark and under Xe lamp and laser illumination.

Photoelectrochemical deposition

According to the CV results a deposition potential ranged from 0.2 to 0.5 V and the deposition time varied from 25 s to 330 s. The deposition transients in Fig. 3.2 and Fig. 3.3 depict the PEC PPy deposition for longer and shorter deposition time, respectively. The film formation can be characterized by three distinct stages (Fig. 3.2). The first part of the PPy deposition transients (A) involves the diffusion-controlled monomer oxidation on the electrode, the second part (B) indicates the nucleation process and the third part (C) consists of a continuous and gradual polymer film growth [187]. It is assumed that the PPy film formation corresponds to the Frank–van der Merwe basic mechanism [188].

The peaks at around 50 s and 150 s in Fig. 3.2 are due to a secondary nucleation which occurs simultaneously with PPy film growth [189]. These peaks are absent in Fig. 3.3 due to the short deposition time. In both, short (Fig. 3.3) and long (Fig. 3.2) deposition time the current density (J) is significantly higher during polymerization under the Xe lamp illumination in comparison to the laser beam illumination due to the difference in light intensity and spectrum (white light from Xe lamp vs. red light from laser). A Xe lamp was particularly chosen for this experiment instead of a halogen lamp due to the following reasons. First, the spectrum of

the Xe lamp is closer to the Sun spectrum and, second, the Xe lamp can be considered as a relatively "cold" source of light as it contains only small portion of an infrared radiation vs. halogen lamp. Conversely, the advantage of using red laser illumination lies in the possibility to selectively deposit PPy onto the a-Si:H surface under low intensity illumination and using a specific wavelength region of light.

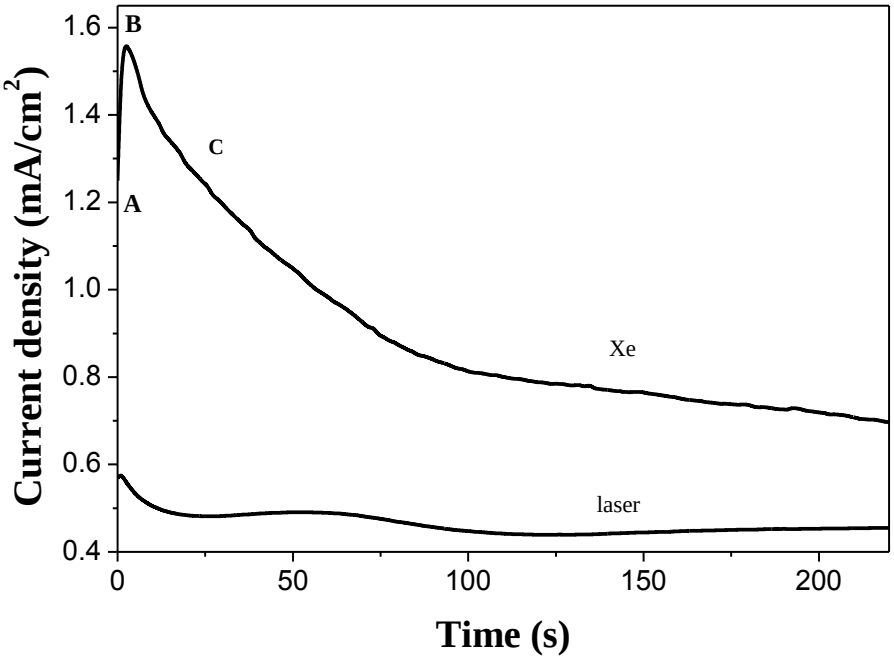

Fig. 3.2. Current density vs. time for potentiostatic electrodeposition (0.5 V) of PPy on i-a-Si:H/n-a-Si:H/AZO/glass electrodes for 220 s in 0.3 M Py/0.1 M NSANa solution under Xe lamp and laser beam illumination.

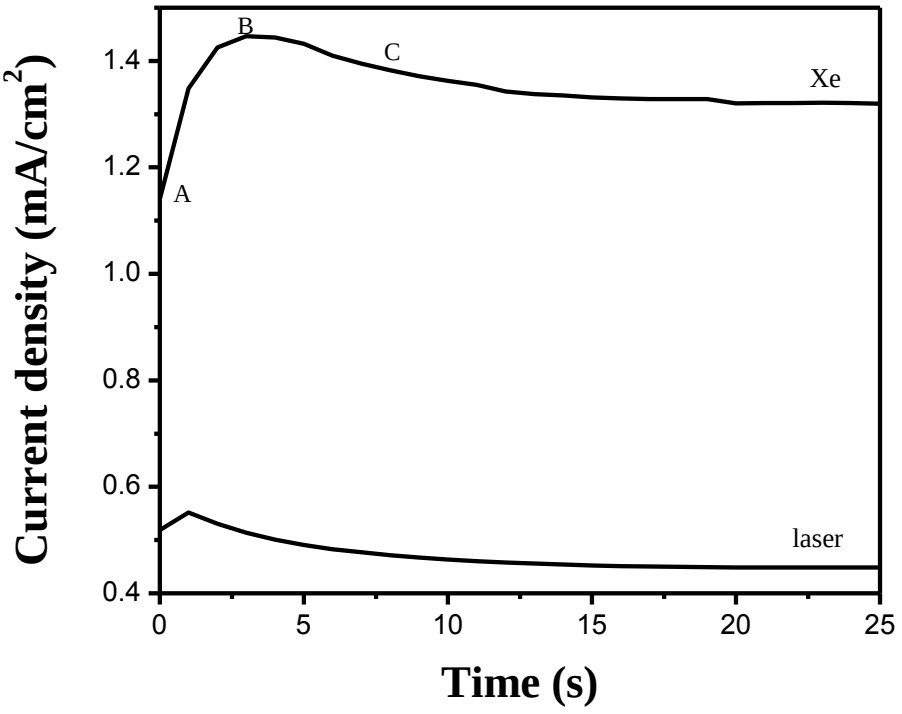

.

Fig. 3.3. Current density vs. time for potentiostatic deposition (0.5 V) of PPy on i-a-Si:H/n-a-Si:H/AZO/glass electrodes for 25 s in 0.3 M Py/0.1 M NSANa solution under Xe lamp and laser beam illumination.

HR-SEM

The cross-sectional HR-SEM micrographs of PPy:NSA/i-a-Si:H/n-a-Si:H/AZO/glass hybrid structures with the PPy functional layer deposited under the Xe lamp illumination, at 0.5 V are shown in Fig. 3.4. The thickness of the a-Si layer for both structures is ca. 400 nm. The border between i-a-Si and n-a-Si:H is invisible since both layers are composed of the same amorphous material with different doping concentration. The visible delamination happens upon breaking the device which is a necessary preparation step for the cross-sectional structure analysis by the HR-SEM. In order to avoid delamination in future nitrogen freezing of the structure before breaking is recommended. The thickness of the PPy:NSA layers deposited for 330 s and 25 s are 300-330 nm and 150-200 nm thick, respectively, for both the red laser and Xe lamp illumination. The PPy:NSA layer is homogenous and adhered to the i-a-Si due to the presence of large anionic organic molecules containing tosyl groups which are a suitable dopant and surface active substance. It can be noted that the PEC deposition of PPy is very sensitive to the surface properties of the substrate. These properties determine the rate of adsorption of Py to the electrode surface at the initial stage, the

distribution of the nucleation centers as well as the charge and potential distribution at the electrode/electrolyte interface [190]. The NSA anionic functional groups induce higher electrical conductivity, improved structural regularity and stability into the polymer chain, which can subsequently more easily adhere at the electrode, enhancing the initial steps of the polymerization process.

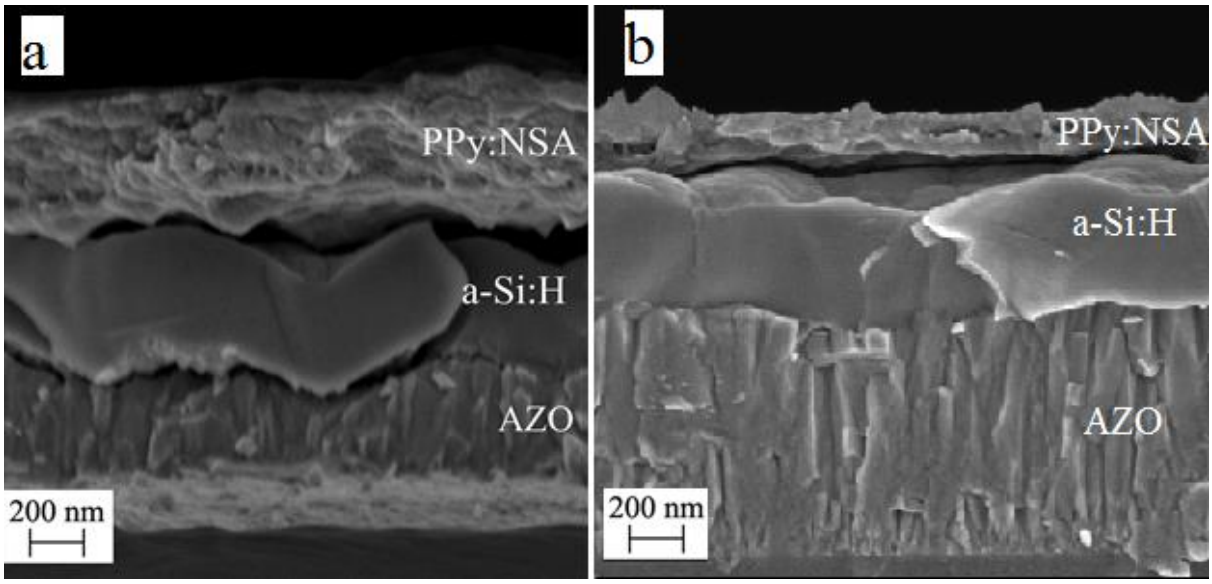

Fig. 3.4. Cross-sectional HR-SEM micrographs of PPy:NSA/i-a-Si:H/n-a-Si:H/AZO/glass structures deposited under the Xe lamp illumination during (a) 330 s and (b) 25 s.

Photoelectrochemical Performance

It was found that the PEC performance of the i-a-Si:H/n-a-Si:H/AZO/glass electrode is enhanced after the electrodeposition of the PPy:NSA film (Fig. 3.5). Enhanced PEC performance is connected to the n-i-p junction formation, which enables hole drift from the i- to p-layer as well as indicates a delay in electron-hole pair recombination. That is confirmed by the transient photocurrent observed for all the examined structures indicating lower recombination losses. The onset potential (V_{on}) value is similar for the a-Si:H structure and the hybrid structure with the PPy film deposited under the laser illumination. It is assumed that a different dopant degree and oxidation states in the PPy layer may affect the PEC performance in Fig.3.5 (b) (c) and (d). This is particularly noticeable in the structure with the PPy layer deposited under Xe lamp illumination (Fig.3.5 (c) and (d)). Here the photoresponse appears in lower potential ranges: a possible effect is a different dopant degree in the PPy layer which is directly connected to the applied conditions of the polymerization process.

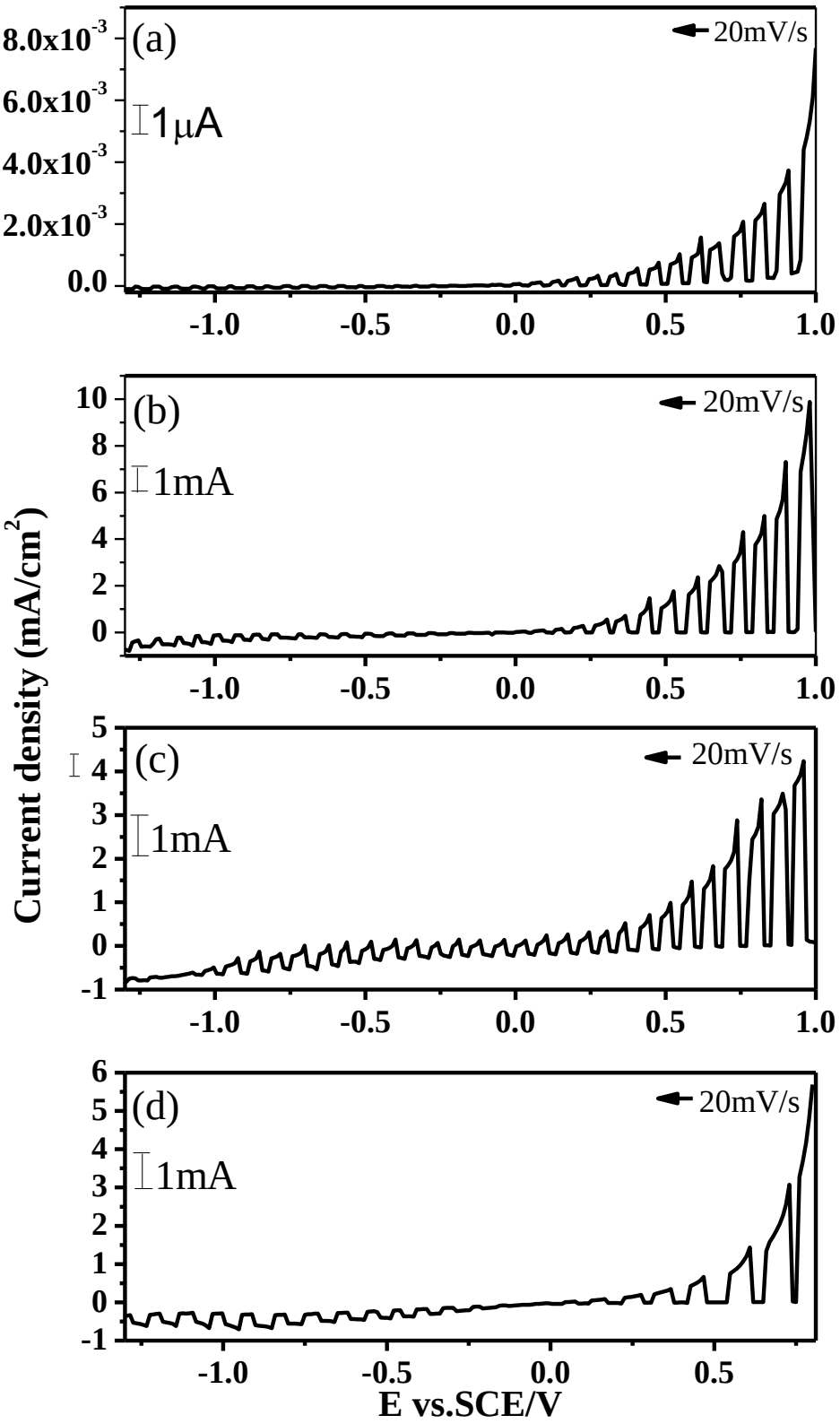

Fig. 3.5. PEC performance of (a) i-a-Si:H/n-a-Si:H/AZO/glass and PPy:NSA/i-a-Si:H/n-a-Si:H/AZO/glass electrodes under chopped white light illumination with PPy layer deposited

previously under (b) laser illumination (300 mV, 330s), (c) Xe lamp illumination (300 mV, 330s) and (d) Xe lamp illumination (200mV, 25s).

The Optical Transmittance and Band Gap

The optical transmittance measurements for PPy:NSA and i-a-Si:H/n-a-Si:H/AZO/glass were recorded in the 300-1100 nm and 300-1500 nm range, respectively, as shown in Fig. 3.6. It can be seen that the transmittance of PPy:NSA deposited under different conditions (i.e. different times) varies depending on the thickness of the polymer layer. The transmittance of the polymer film deposited for 25 s is over 90%, whereas that of the PPy:NSA layer deposited for 40 s is around 80-93%. The transmittance decreases significantly to approximately 25% with a thicker polymer film deposited at long deposition time of 330 s. The fundamental absorption edge was found to be at around 300- 350 nm above which all the curves exhibit oscillatory behavior, which might be a result of interference phenomena between two surfaces of the PPy:NSA film and ITO.

The transmittance of the i-a-Si:H/n-a-Si:H/AZO/glass structure is $\geq$ 55 % as shown in Fig. 3.6 (b). The T verus λ measurements showed two band edges at approximately 550-650 nm and 650-750 nm which correspond to the transmittance of approximately 15% and 30%, respectively. The two band edges of i-a-Si:H/n-a-Si:H/AZO/glass may be explained as following: the i-a-Si:H/n-a-Si:H/AZO/glass is composed of two a-Si layers; i.e. intrinsic (undoped) and n-doped (phosphorus doping) layer. Above these, the curve also exhibits oscillatory behaviour, which might be a result of the interference phenomena between the surfaces of the i-a-Si:H/n-a-Si:H/AZO/glass structure. The estimated band edge at ca. 1.7 eV might therefore correspond to highly doped n-a-Si:H layer whereas at ca. 1.9 eV corresponds to the i-a-Si:H layer with possible contamination/diffusion of phosphorus. According to literature the doping of a-Si:H shifts the absorption curves to lower energies, causing a decrease of the energy band gap. In i-a-Si:H, high band gap (ca. > 2 eV) can be reached while in n-a-Si:H the phosphorus doping decreases the energy band gap to ca. 1.7 eV [191]. The other possible explanation of two band edges is the presence of other defects or/and oxide layer [192] present on the top of i-Si:H which create sub band gap absorption.

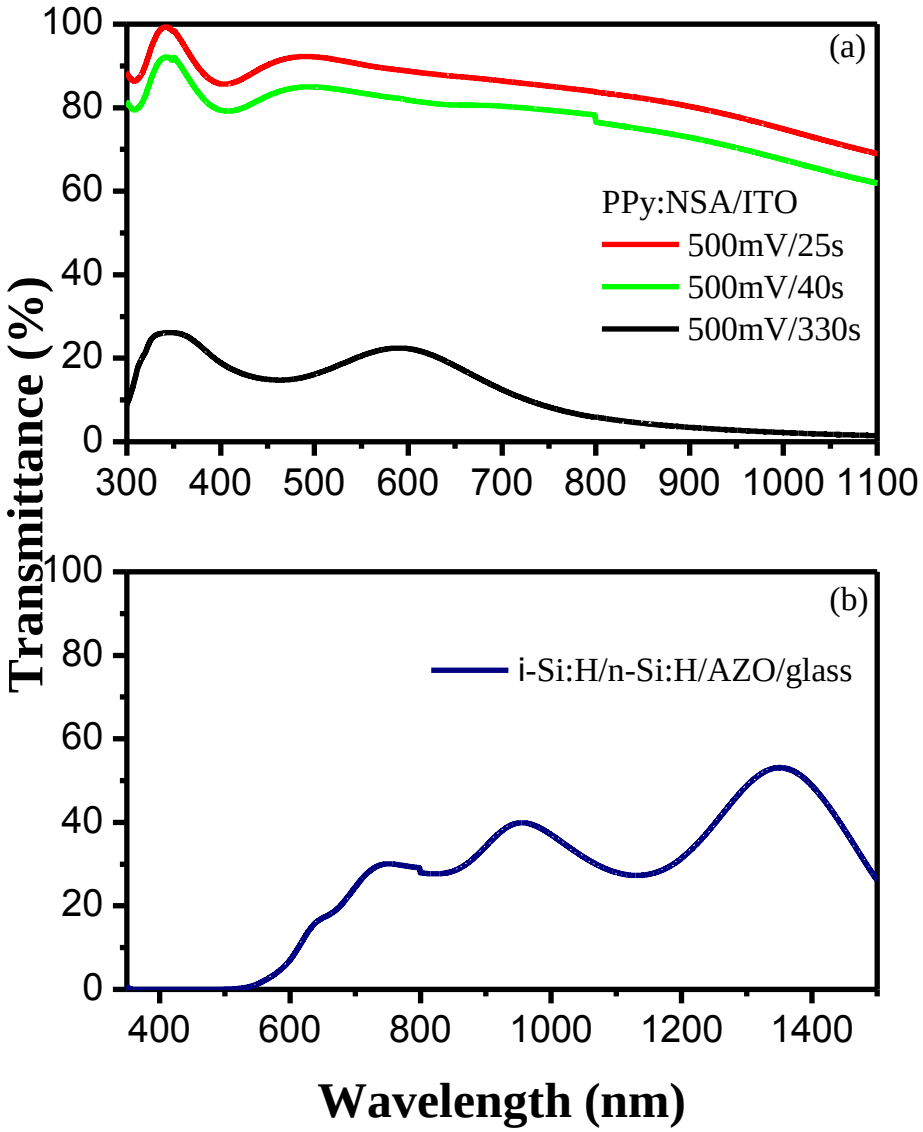

Fig. 3.6. UV-Vis transmittance spectra for (a) PPy:NSA deposited at different times and (b) i-a-Si:H/n-a-Si:H/AZO/glass substrate.

The energy band gap of PPy:NSA was estimated by the extrapolation of the linear portion on the energy (hν) axis and taking the intercept (see Experimental section- UV-Vis spectrophotometry) (Fig. 3.7). The optical band gaps of PPy:NSA deposited on ITO at 25 s and 40 s were determined to be 3.78 eV and 3.72 eV, respectively (Fig. 3.7). These values agree with literature [193-196]. This small change in the band gap as a function of deposition time may be due to different phase/composition, crystallinity, level of doping of the PPy:NSA film, oxidation, length of polymer chain and the presence of bipolarons.

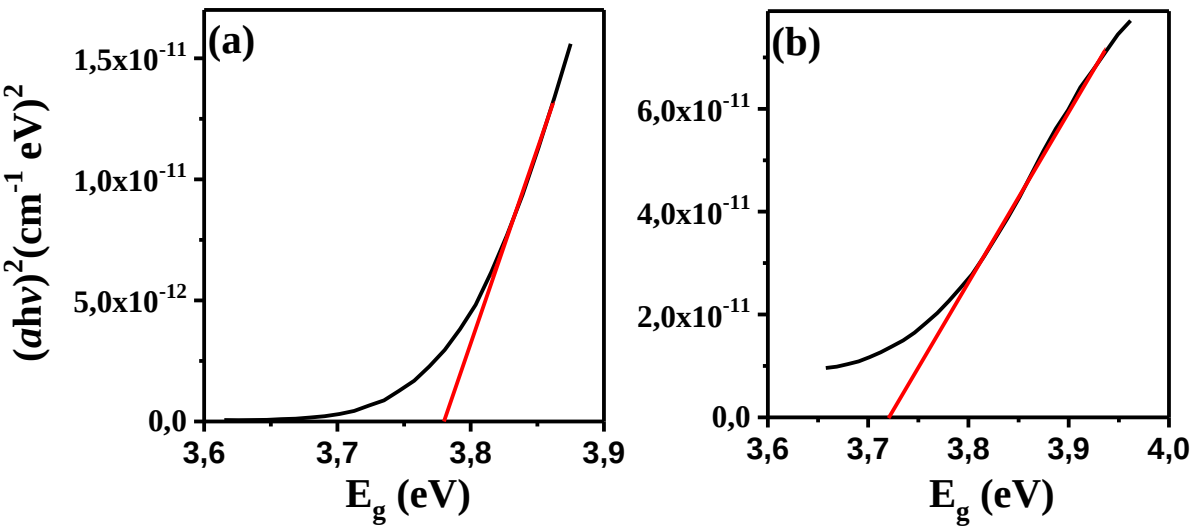

Fig. 3.7. Tauc's plots for PPy:NSA deposited on ITO at 0.5 V for (a) 25 s and (b) 40 s.

Kelvin Probe Measurements

Kelvin probe measurements have been applied to inorganic i-a-Si:H/n-a-Si:H/AZO/glass and hybrid PPy:NSA/i-a-Si/n-a-Si:H/AZO/glass structures (Fig. 3.8). SP for i-a-Si:H/n-a-Si:H/AZO/glass in dark was measured to be ca. 450 mV, whereas under the red laser irradiation it increased up to ca. 670 mV (Fig. 3.8, a). SP of the PPy:NSA/i-a-Si:H/n-a-Si:H/AZO/glass structure (200 mV, 25 s) increased under red light illumination from 120 mV to ca. 150 mV as shown in Fig. 3.8 (b). SP of the PPy:NSA/i-a-Si:H/n-a-Si:H/AZO/glass structure with PPy layer deposited at higher potential of 500 mV is estimated to be approximately 25 mV (Fig. 3.8, c). Under red laser light irradiation, SP increased to ca. 225 mV. The SP of i-a-Si/n-a-Si:H/AZO/glass structure in dark conditions has the highest value in comparison with complete hybrid PPy:NSA/i-a-Si:H/n-a-Si:H/AZO/glass structures. In addition, as seen in Fig. 3.8 (b) and (c) the SP varies for different deposition conditions of the PPy:NSA layer. It is assumed that this difference is attributed to different phases/crystallinity of the PPy:NSA layer and different doping level which depends directly on the deposition conditions (i.e. 500 mV vs. 200 mV). Also due to optical properties PPy shouldn't have a photoresponse under red light. The photoresponse of the hybrid structure is explained by the influence of Si layer under the PPy:NSA layer.

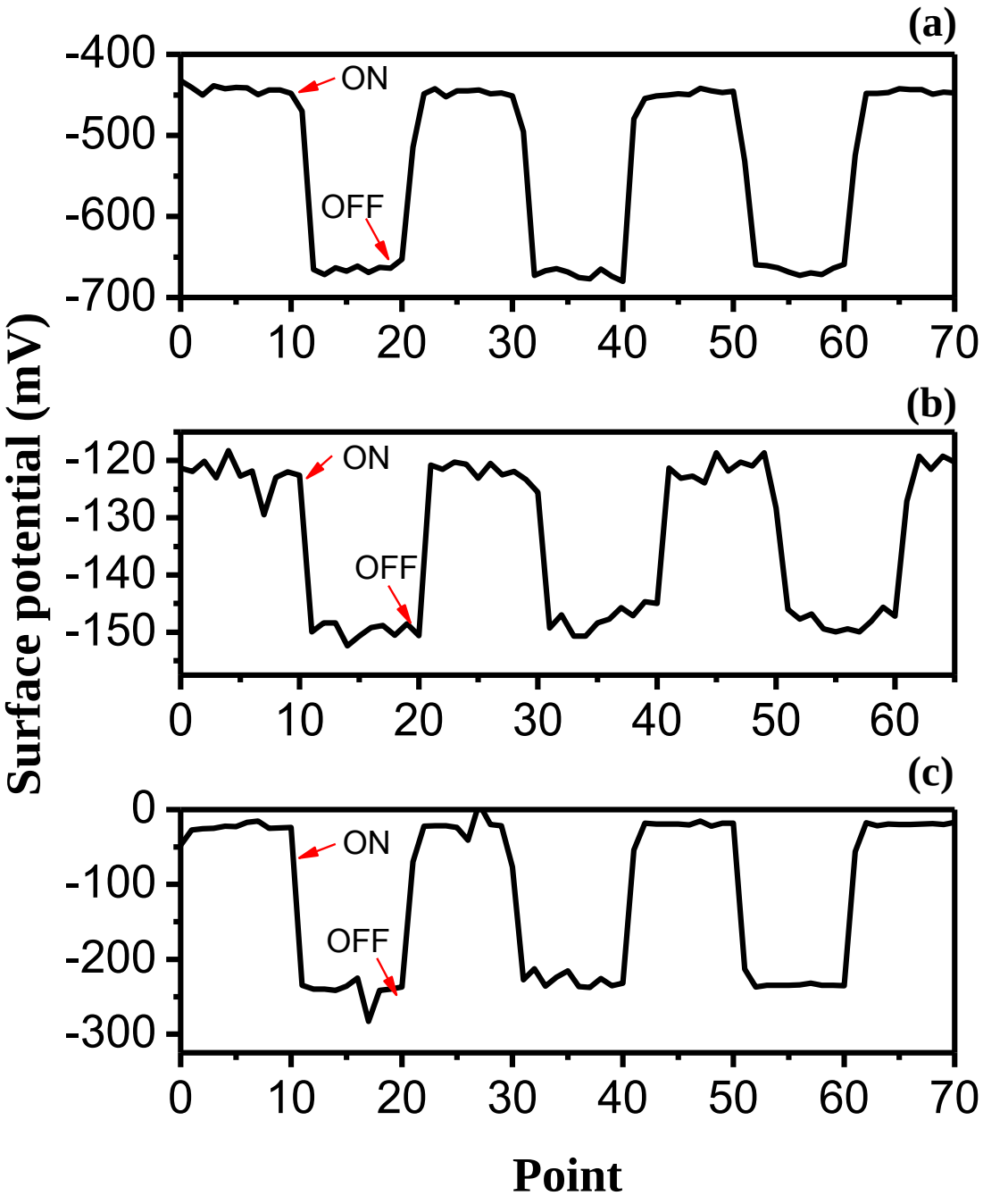

Fig. 3.8. Kelvin probe measurements of i-a-Si/n-Si:H/AZO/glass structure (a) without PPy and, with PPy layer deposited for 25 s at (b) 200 mV and (c) 500 mV under the chopped red laser illumination.

According to the solid-state J-V measurements, complete hybrid structures with the PPy film deposited at potential values from 0.2 V to 0.5 V during 220 -330 s demonstrated the

best PV performance (Fig. 3.9). It should be noted that the obtained J-V parameters were comparable for both graphite and Au contacts. However, hybrid structures with the PPy:NSA functional layers deposited under red laser illumination showed higher fill factor (FF) of 50-56% (D6 and D16 structures: Table. 1.). On the other hand, hybrid structures with the PPy:NSA functional layer deposited for short deposition time (25 -50 s) demonstrated so-called roll-over effect which gives the J-V curve a characteristic S-shape (Fig.3.10). In general, the roll-over shape is a result of a back diode presence in series with the main junction photodiode and as a consequence V_{OC} and FF degrade. However there are other factors affecting the S-shape of the J-V curves: (a) high energy barriers due to misaligned electrode WF [197-199], (b) hole blocking properties of the hole transport layer [200] and (c) dopant contamination [201] or dopant diffusion into functional layers [202]. In the case of our structures the roll-over effect in the third and fourth quadrant is thought to be a result of the back diode presence at the PPy:NSA/i-a-Si:H interface.

The J-V parameters of the complete hybrid structures were considerably lower for structures with the PPy:NSA layer electrodeposited for short times. The best J-V parameters achieved in this series were obtained using the Xe lamp illumination; yet again the J-V parameters were comparable for both graphite and Au contact.

It can be concluded that the red laser illumination is more suitable for longer deposition time. As the laser intensity is too low to achieve comparable J-V characteristics of structures with PPy deposited during short times. However, the Xe lamp is suitable for the short time deposition, enabling homogenous deposition and good adhesion of the PPy layer on the i-a-Si/n-a-Si:H/AZO/glass structure (Fig 3.4).

The highest PCE of 2.71% was obtained for the Au/PPy:NSA/i-a-Si/n-a-Si:H/AZO/glass structure with the PPy:NSA film deposited under the red laser illumination, at the potential of 300 mV for 200 s (Table 3.1).

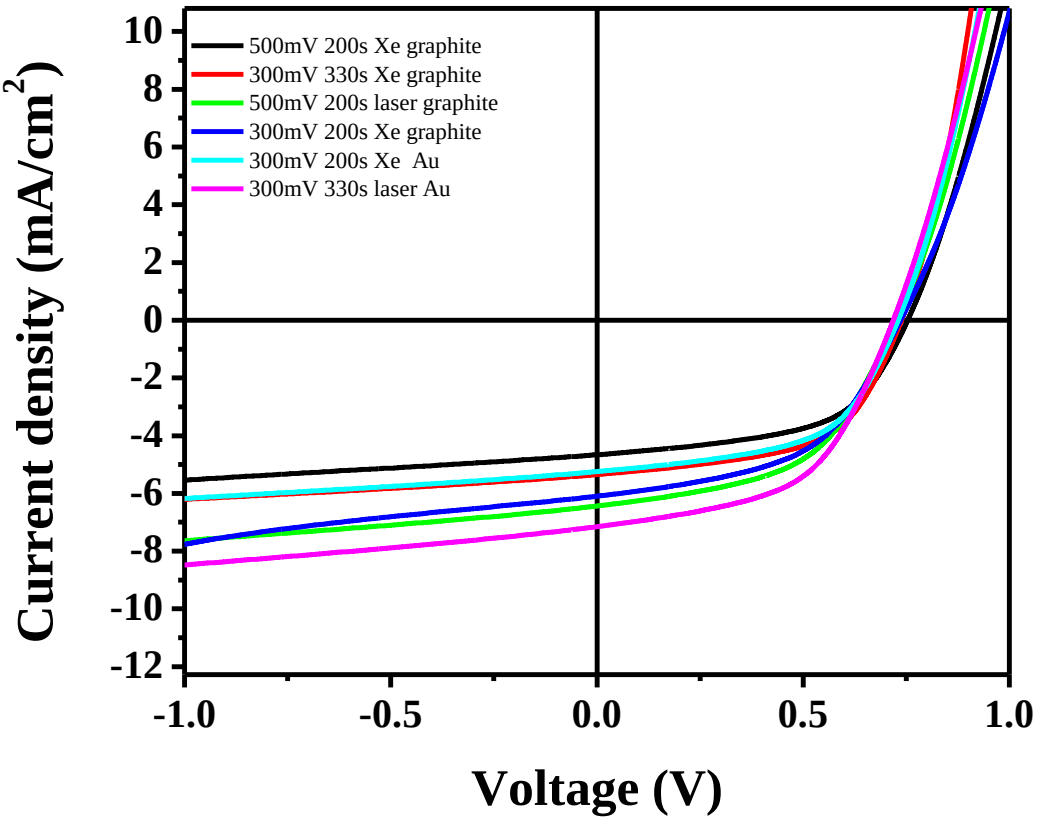

Fig. 3.9. J-V characteristics of the Au/PPy/i-a-Si/n-a-Si:H/AZO/glass and graphite/PPy/i-a-Si:H/n-a-Si:H/AZO/glass structures under white light illumination of 100 mW/cm^2 intensity (long deposition time).

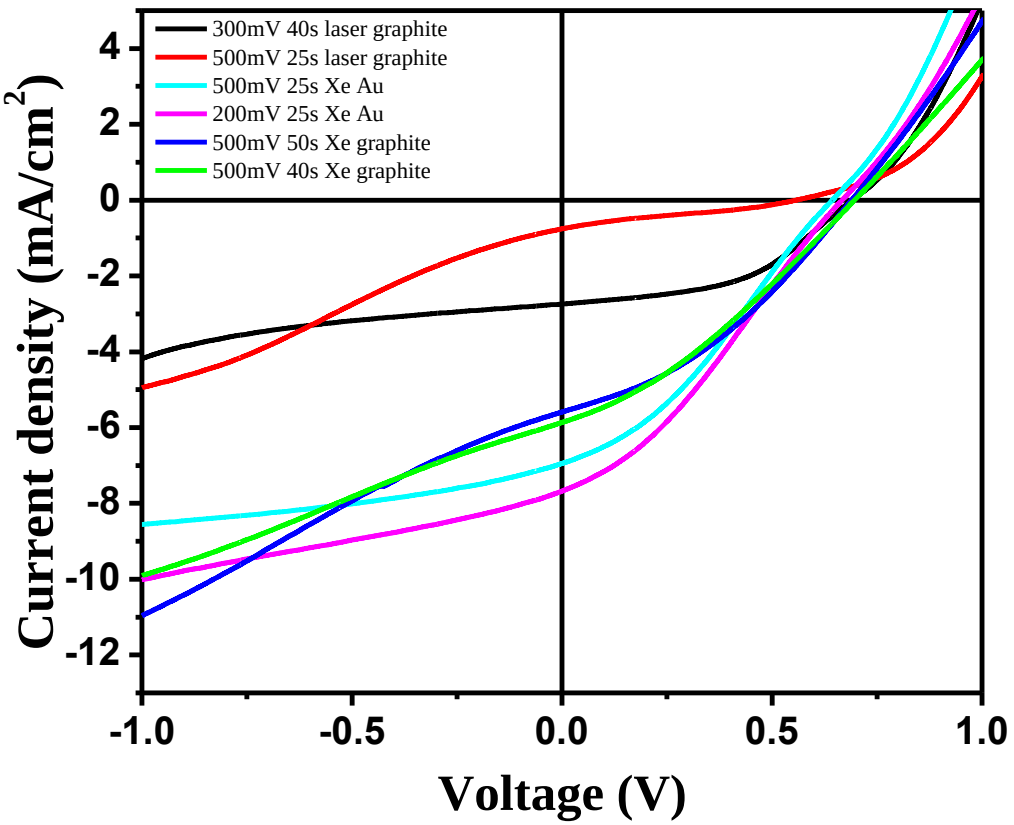

Fig. 3.10. J-V characteristics of the Au/PPy/i-a-Si/n-a-Si:H/AZO/glass and graphite/PPy/i-a-Si:H/n-a-Si:H/AZO/glass structures under white light illumination of 100 mW/cm^2 intensity (short deposition time).

The photoconversion efficiency (PCE) of the unencapsulated complete hybrid structures kept in a silica gel desiccator for one year decreased by approximately 13%. After following 24 hour Xe lamp illumination of 100 mW/cm^2 intensity in ambient conditions the efficiency further decreased on average by 22%. Further investigations should be carried out in order to determine and understand the degradation mechanism

It should be noted that significantly lower values of the structures with short deposition times were possibly obtained due to the quality difference of the a-Si:H substrates.

Table 3.1 PV parameters of the prepared hybrid structures

ECP:dopant	Conditions	V_{oc} (mV)	J (mA/cm^2)	FF (%)	η (%)	S (cm^2)
Short deposition times						
PPY:NSA (#4)	300mV, 40s, laser, graphite	691.34	2.7	47.2	0.9	0.196
PPy:NSA (#7)	500mV, 25s, laser, graphite	558.31	0.8	26.1	0.2	0.196
PPy:NSA*	500mV, 25s, Xe, Au	643.20	7.0	33.0	1.5	0.196
PPy:NSA*	200mV, 25s, Xe, Au	667.00	7.7	31.1	1.6	0.196
PPy:NSA (#2)	500mV, 50s, Xe, graphite	689.68	5.6	35.7	1.4	0.071
PPy:NSA (#3)	500mV,40s,Xe,graphite	696.59	5.9	32.0	1.3	0.096
Long deposition times						
PPy:NSa (D3)	500mV,200s, Xe,graphite	753.80	4.7	55.1	1.9	0.196
PPy:NSA (D4)	300mV, 330s, Xe,graphite	738.80	2.7	56.6	1.1	0.196
PPy:NSA (D6)	500mV,200s,laser,graphite	727.00	6.4	51.4	2.4	0.196
PPy:NSA (D7)	300mV,200s,Xe,graphite	736.40	6.1	50.6	2.3	0.196
PPy:NSA (D6)	300mV,200s, Xe,Au	730.50	3.9	55.4	1.6	0.196
PPy:NSA(D16)	300mV,200s,laser,Au	719.00	7.2	52.6	2.7	0.196

*unlimited

Chapter IV: Conclusions

The main aim of this work was to fabricate and investigate novel hybrid structures based on PPy:NSA deposited photoelectrochemically onto photoactive i-a-Si:H/n-a-Si:H/AZO/glass electrode.

It was found that polymerization of Py onto the i-a-Si:H surface can be enhanced by the assistance of light and performed at reduced oxidative potential values starting from as low as 0.2 V. The deposition curves clearly showed the importance of light illumination. The difference in the current density is explained by various light intensity.

Resulting PPy films demonstrated good coverage of the i-a-Si:H surface and uniformity throughout the surface as shown by the HR-SEM graphs. The thickness of the PPy films was also shown to be dependent on the deposition time.

The PEC performance of the i-a-Si:H/n-a-Si:H/AZO/glass electrode enhanced after the PPy film which completes the SC structure. The optical band gap of PPy:NSA thin films with different time intervals was found to be in a range of 3.7 - 3.8 eV.

The PCE values for the complete PPy/i-a-Si:H/n-a-Si:H/AZO/glass structures were comparable with respect to the applied potential range and back contacts. However, the difference lies in the deposition times connected to a particular illumination source. Laser illumination appears to be more suitable for long deposition times whereas Xe lamp illumination is more appropriate for short deposition times.

The PCE value for the best obtained structures is 2.71% for structures deposited using laser illumination at potential value of 300 mV and during 220 s. However, optimization of the interface between the a-Si:H and ECP layers is likely to improve the cell performance further. It should be noted that obtained PCE value was relatively high for hybrid structures based on the a-Si photo-absorber. The PEC deposition method with reduced applied potentials and the use of well-studied materials such as a-Si and doped PPy make these hybrid devices a promising alternative to existing hybrid SC.

Resumé

Compared to today's consumption, the yearly consumption of solar energy would have to increase by two orders of magnitude by the year 2050 in order to achieve sustainable goals set up in the Paris agreement. At the same time, the costs of sustainable technologies needs to be decreased in order to allow competition with fossil fuels and achieve economical sustainability.

While the production processes cost can be reduced, the supply of raw materials, in particular scarce materials such as In or Te, remains an open issue. Only a reduced payback time will lead to a wide spread of PV systems necessary to meet the targets in reducing greenhouse gases. One possibility is to use abundant materials such as a-Si and ECPs applied to flexible and light substrate material to decrease the overall price of the PV module.

a:Si can be obtained at low-cost in comparison with c:Si. The required deposition process can take place at low temperatures (typically between 150° and 200°C) therefore saving the cost and allowing the usage of low-temperature substrates. Thin film a:Si cells also offer the advantage of a comparatively stable technology in contact with oxygen, moisture and UV-light. Additionally, vacuum-free low-temperature technology of their fabrication makes these materials low-cost materials in flexible optoelectronic and electronic devices.

Another example is the use of thin film ECPs allowing the elimination of expensive materials and technologies while reducing the thickness of SCs and therefore improving their flexibility.

Compared to current technologies on the market the investigated hybrid solar cell based on ECP and a-Si eliminates toxic and/or scarce materials such as Cd, Te or In. This leads to significantly enhancing recyclability and eliminating extra costs.

The main aim of this thesis is to investigate novel n-i-p heterostructure based on a:Si and photoelectrochemically deposited ECP PPy. For SC applications, heterojunctions are highly interesting structures since two materials are stacked together to form an electronic device of unique properties and thus the interface between the materials can be used to optimize the electrical performance. One of the most important issues is the electronic band offset between the two materials which has a major impact on the defect structure and thus on the loss mechanism. New SC concepts can be implemented with higher efficiency potential: a loss free heterocontact with high V_{oc} in the SC.

In this study the ECP film was deposited using photoelectrochemical deposition under varying conditions such as applied potential and time. These structures were investigated and characterized.

The PCE value for the best obtained structures was around 2.7% for structures deposited using laser illumination at a potential value of 300 mV and at long deposition times (220 s). The photoelectrochemical deposition method with reduced applied potentials and the use of well-studied abundant materials such as a-Si and PPy make these hybrid devices a promising alternative to the current hybrid PV.

Kokkuvõte

Selleks, et saavutada 2050. aastaks Pariisi kokkuleppes seatud sihtmärke kliima soojenemise pidurdamiseks, peab päikeseenergia kasutamine tänasega võrreldes kasvama kahe suurusjärgu võrra. Samaaegselt peab taastuvenergia lahenduste kulukus vähenema selleks, et konkureerida fossiilkütustega ning saavutada majanduslik jätkusuutlikkus.

Kuigi tootmisprotsessi kulusid on võimalik vähendada, on toormaterjali tarne, eriti haruldaste materjalide nagu indium või telluur, endiselt probleemne. Selleks, et päikeseelemendid leviks sel hulgal, et jõuda kasvuhoonegaaside vähendamise sihtmärkideni, peab nende tasuvusperiood vähenema. Üks võimalus vähendada päikesemooduli hinda tervikuna on kasutada kergel ja painduval alusel rikkalikult leiduvaid materjale nagu amorfne räni (Si) ja elektit juhtivad polümeerid.

Amorfse Si tootmine on vähem kulukam, kui kristallilise Si. Selleks vajalikku sadestusprotsessi on võimalik viia läbi madalal temperatuuril (üldiselt 150°C ja 200°C vahemikus), mis võimaldab omakorda kasutada ka aluseid, mis ei talu kõrgeid temperatuure. Õhukesed amorfse Si paneelid on stabiilsed hapniku, niiskuse ja UV valgusega kontaktis. Nende madalatemperatuuriline ja vaakumivaba tootmismeetod teeb need materjalid võrdlemiselt odavaks alternatiiviks painduvate optoelektrooniliste ja elektrooniliste seadmete tootmiseks.

Lisaks õhukeste juhtivate polümeerkihtide kasutamine võimaldab toota õhemaid paneele, mis omakorda parandab nende paindlikkust.

Võrreldes hetkel saadalolevate lahendustega likvideerib uuritud juhtivpolümeeridel ja amorfsel Si-l põhinev hübriidpaneel toksiliste ja haruldaste materjalide vajalikkuse - sealhulgas Cd, Te või In. See omakorda tähendab, et tulenevad paneelide lihtsamat taasringlussevõttu ja lisakulude vähenemist.

Antud lõputöö peamine eesmärk on uurida uudset n-i-p heterostruktuuri, mis baseerub amorfsel Si-l ja fotoelektrokeemiliselt sadestatud polüpüroolil. Heterosiirded on ülimalt huvitavad struktuurid päikesepaneelides kasutamiseks kuivõrd kahe materjali kihistamisest tuleneva elektrilise seadme omadused on ainulaadsed ning kahe materjali vahelist ühendust on võimalik kasutada tootlikuse optimiseerimiseks. Siinjuures on üheks peamiseks probleemiks kahe materjali keelutsoonide nihe, millel on suur mõju struktuuri defektidele ja nendest tulenevale tootlikuse langusele. Uusi päikesepaneelide lahendusi on võimalik

rakendada suurema efektiivsuse potentsiaaliga võttes kasutusele nullkaotusega heterokontakti kõrge Voc-ga paneelis.

Antud uuringus sadestati juhtivpolümeeri kiht fotoelektrokeemilise meetodiga erinevatel tingimustel - muutes potentsiaali ja aega. Seejärel uuriti ja iseloomustati valmistatuid struktuure.

Parimate struktuuride effectiivsuse väärtus oli ligi 2.7% laservalguse all sadestatud struktuuride puhul, kus potentiaali suurus oli 300 mV ja kasutatati pikka sadestusaega (220 s). Mainitud fotoelektrokeemiline sadestusmeetod, vähendatud potentsiaalil ja rikkalikult leiduvate materjalide kasutamine, nagu a-Si ja PPy, teevad antud hübriidsetest elementidest paljulubava alternatiivi hetkel kasutusel olevatele hübriidsetele päikesepatereidele.

Reference

[1] Special Report on Renewable Energy Sources and Climate Change Mitigation, Intergovernmental Panel on Climate Change (2011).

[2] Blakers, A., Zin, N., Mcintosh, K. R., & Fong, K. (2013) High Efficiency Silicon Solar Cells. Energy Procedia, 33, 1-10.

[3] Meillaud, F., Boccard, M., Bugnon, G., Despeisse, M., Hänni, S., Haug, F., Ballif, C. (2015). Recent advances and remaining challenges in thin-film silicon photovoltaic technology. Materials Today, 18(7), 378-384.

[4] Chopra, K. L., Paulson, P. D., & Dutta, V. (2004). Thin-film solar cells: An overview. Progress in Photovoltaics: Research and Applications,12(23), 69-92.

[5] Charles, H., & Ariotedjo, A., Review of amorphous and polycrystalline thin film silicon solar cell performance parameters. Solar Energy (1980) 329-339.

[6] Cabarrocas, P. R., Plasma enhanced chemical vapor deposition of amorphous, polymorphous and microcrystalline silicon films. Journal of Non-Crystalline Solids, (2000) 266-269, 31-37.

[7] Shah, A., Meier, J., Buechel, A., Kroll, U., Steinhauser, J., Meillaud, F., Dominé, D, Towards very low-cost mass production of thin-film silicon photovoltaic (PV) solar modules on glass, Thin Solid Films (2006) pp.292-299.

[8] Geißendörfer, S., Theuring, M., Titz, M., Mogck , S., Pflaum, C., Abebe , B. T., Schütze, F., Wynands, D., Kirstein, U., Schweitzer, A., Steenhoff, V., Neumüller, A., Borzutzki, Nowak, R.E.K., Philipp, A., Klement, P., Sergeev, O., Vehse, M., Maydell, M. (2015) The SiSoFlex Project: Silicon Based Thin-Film Solar Cells on Flexible Aluminium Substrates, Next Energy

[9] Alpuim, P., Samantilleke, A., Marins, E., Oliveira, F., Cerqueira, M. F., Rebouta, L., Bourée, J., Amorphous silicon thin-film solar cells deposited on flexible substrates using different zinc oxide layers. Physica Status Solidi (c) (2010).

[10] Luque, A., & Hegedus, S. (2003). Handbook of photovoltaic science and engineering, pg. 5050-542, Hoboken, NJ: Wiley.

[11] Chandrasekaran, J., Nithyaprakash, D., Ajjan, K., Maruthamuthu, S., Manoharan, D., & Kumar, S, Hybrid solar cell based on blending of organic and inorganic materials—An overview, Renewable and Sustainable Energy Reviews (2011) pp.1228-1238.

[12] Wright, M., & Uddin, A., Organic—inorganic hybrid solar cells: A comparative review, Solar Energy Materials and Solar Cells (2012) pp.87-111.

[13] A.M. Funde, A.G. Nasibulin, H.G. Syed, A.S. Anisimov, A. Tsapenko, P. Lund, J.D. Santos, I. Torres, J.J. Gandía, J. Cárabe, A.D. Rozenberg, I.A. Levitsky, Carbon nanotube – amorphous silicon hybrid solar cell with improved conversion efficiency, Nanotechnology (2016) pp. 185401.

[14] M.H. Yun, J.H. Jang, K.M. Kim, H. Song, J.C. Lee, J.Y. Kim, A hybrid solar cell fabricated using amorphous silicon and a fullerene derivative, Physical Chemistry Chemical Physics (2013) pp. 19913.

[15] N.T. Kalyani, S. Dhoble, Organic light emitting diodes: Energy saving lighting technology—A review, Renewable and Sustainable Energy Reviews (2012) pp. 2696-2723.

[16] A. Neumüller, O. Sergeev, M. Vehse, C. Agert, Argon Plasma Treatment at the i-/p-Interface in Silicon Thin-Film Solar Cells and its Influence on the Light Induced Degradation, Energy Procedia (2015) pp.242-250.

[17] D. Natali, M. Caironi, Photodetectors: materials, devices and applications, Cambridge: Woodhead Publishing (2016) Chapter 7: Organic photodetectors, pp.195-254.

[18] C. Reese, M. Roberts, M. Ling, Z. Bao, Organic thin film transistors. Materials Today (2004) pp. 20-27.

[19] R. Balint, N.J. Cassidy, S.H. Cartmell, Conductive polymers: Towards a smart biomaterial for tissue engineering, Acta Biomaterialia (2014) pp. 2341-2353.

[20] D. Kaduwal, B. Zimmermann, U. Würfel, ITO-free laminated concept for flexible organic solar cells, Solar Energy Materials and Solar Cells (2014) pp.449-453.

[21] Wikipedia, Polypyrrole (2017) URL:https://en.wikipedia.org/wiki/Polypyrrole.

[22] G.M. Kumar, V. Raman, J. Kawakita, P. Ilanchezhiyan, R. Jayavel, Fabrication of polypyrrole/ZnCoO nanohybrid systems for solar cell applications. Dalton Transactions (2010) pp. 8325.

[23] O. Inganäs, T. Skotheim, I. Lundström, Schottky Barrier Formation Between Polypyrrole and Crystalline and Amorphous Hydrogenated Silicon, Physica Scripta (1982) pp. 863-867.

[24] E.L. Williams, G.E. Jabbour, Q. Wang, S.E. Shaheen, D.S. Ginley, E.A. Schiff, Conducting polymer and hydrogenated amorphous silicon hybrid solar cells, Applied Physics Letters (2005) pp. 223504.

[25] Street, R. A. Hydrogenated amorphous silicon. Cambridge: Cambridge University Press, (2005) ISBN 0-521-37156-2.

[26] J.A. Reimer, M.A. Petrich, Structural Heterogeneities in Device-Quality Amorphous Hydrogenated Semiconductors, Amorphous Silicon and Related Materials (1989), pp. 3-27.

[27] A. Luque, S. Hegedus, Handbook of photovoltaic science and engineering. Chichester, West Sussex, U.K.: Wiley (2003) pp.514, Fig. 12.7, ISBN 0-471-49196-9.

[28] W. B. Jackson, C. C. Tsai, R. Thompson. Diffusion of paramagnetic defects in amorphous silicon, Physical Review Letters (1990) pp.56-59.

[29] D. L Staebler, C. R. Wronski, Reversible conductivity changes in discharge□produced amorphous Si, Applied Physics Letters (1977) pp. 292-94.

[30] A. Luque, S. Hegedus, Handbook of photovoltaic science and engineering, Amorphous Silicon-Based Solar Cells, Chichester, West Sussex, U.K.:Wiley (2003) ISBN 0-471-49196-9.

[31] G. Qing, Q. Wang, E.A. Schiff, Y.M. Li, C.T. Malone, Hole drift mobility measurements in amorphous silicon carbon alloys, Journal of Applied Physics, vol.76 (1994) pp.2310-315.

[32] Q. Wang, H. Antoniadis, E. A. Schiff, S. Guha, Electron-drift-mobility measurements and exponential conduction-band tails in hydrogenated amorphous silicon-germanium alloys, Physical Review B (1993) pp.9435-448.

[33] N.F. Mott, Conduction in non-crystalline materials, Oxford: Clarendon press (1993) ISBN: 9780198539797.

[34] "Band gap." Wikipedia (Accessed 22nd February 2017).

[35] I.S. Chen, T. N. Jackson, C. R. Wronski, Characterization of semiconductor heterojunctions using internal photoemission, Journal of Applied Physics (1996) pp.8470-474.

[36] A. Rockett, The Materials Science of Semiconductors, Amorphous Semiconductors, Springer (2008) ISBN: 978-0-387-25653-5.

[37] T. Hama, H. Okamoto, Y. Hamakawa, T. Matsubara, Hydrogen content dependence of the optical energy gap in a-Si:H, Journal of Non-Crystalline Solids (1983) pp.333-36

[38] S. Guha, J. Payson, S. Agarwal, S. Ovshinsky, Fluorinated amorphous silicon-germanium alloys deposited from disilane-germane mixture, Journal of Non-Crystalline Solids (1987) pp.1455-458.

[39] R.C. Chittick, J.H. Alexander, H.F. Sterling, The Preparation and Properties of Amorphous Silicon, Journal of the Electrochemical Society (1969) pp.77-81.

[40] S. Guha, J. Yang, A. Banerjee, T. Glatfelter, K. Hoffman, S. R. Ovshinsky, M. Izu, H. C. Ovshinsky, X. Deng, Amorphous Silicon Alloy Photovoltaic Technology - From R&D to Production, MRS Proceedings (1994).

[41] R.R. Arya, D. E. Carlson, Amorphous silicon PV module manufacturing at BP solar, Progress in Photovoltaics: Research and Applications (2002) pp.69-76.

[42] H. Curtins, N. Wyrsch, A. Shah, High-rate deposition of amorphous hydrogenated silicon: effect of plasma excitation frequency, Electronics Letters (1987) pp.228-30.

[43] M.N. Jeon, K. Kamisako, Hydrogenated Amorphous Silicon Thin Films as Passivation Layers Deposited by Microwave Remote-PECVD for Heterojunction Solar Cells, Transactions on Electrical and Electronic Materials (2009) pp.75-79.

[44] R. Schropp, Industrialization of Hot Wire Chemical Vapor Deposition for thin film applications, Thin Solid Films (2015) pp.272-83.

[45] K.O. Kamisako, K. Aota, Y. Tarui, Analysis of Deposition Rate Distribution in the Photo-CVD of a-Si by a Unified Reactor with a Lamp, Japanese Journal of Applied Physics (1984).

[46] W. Paul, A.J. Lewis, G.A.N. Connell. , T.D. Moustakas, Doping, Schottky barrier and junction formation in amorphous germanium and silicon by RF sputtering, Microelectronics Reliability (1977) pp.215.

[47] R.W. Collins, Hydrogenated amorphous silicon alloy deposition processes, Journal of Non-Crystalline Solids (1994) pp.210-13.

[48] R.E.I. Schropp, M. Zeman, Amorphous and Microcrystalline Silicon Solar Cells Modeling, Materials and Device Technology. Springer Verlag (2014) ISBN: 978-1-4615-5631-2.

[49] Current injection technique, Wikipedia (2016), Accessed February 22, 2017.

[50] H. Sai, T. Matsui, K. Matsubara, Stabilized 14.0%-efficient triple-junction thin-film silicon solar cell, Applied Physics Letters (2016) pp.183506.

[51] S. Beaupré, M. Leclerc, PCDTBT: en route for low cost plastic solar cells, Journal of Materials Chemistry A (2013) pp.11097.

[52] S. Guenes, Serap, H.Neugebauer, N. S. Sariciftci, Conjugated Polymer-Based Organic Solar Cells, Chemical Review (2007) pp.1324−1338.

[53] A. Facchetti, Polymer donor–polymer acceptor (all-polymer) solar cells, Materials Today (2013) pp.123-32.

[54] H.S. Nalwa, Handbook of Conductive Molecules and Polymers, John Wiley & Sons Ltd.: Chichester (1997) Vols. 1-4.

[55] Conductive polymer, Wikipedia. February 15, 2017, (Accessed 27th February 2017).

[56] D. Liming, Intelligent macromolecules for smart devices: from materials synthesis to device applications, Conductive Polymers, London: Springer-Verlag (2010) ISBN 978-1-85233-849-7.

[57] H. Hoppe, N.S. Sariciftci , Organic solar cells: An overview, Journal of Materials Research (2004) pp. 1924-1945.

[58] P. A. Lane, J. Rostalski, C. Giebeler, S.I. Martin, D.D.C. Bradley, D. Meissner, Electroabsorption studies of phthalocyanine/perylene solar cells, Solar Energy Materials and Solar Cells (2000) pp.3-13.

[59] Sigma bonds of ethylene, Media Portfolio (Accessed 27th February 2017).

[60] J. Nelson, Organic photovoltaic films, Materials Today (2002) pp. 20-27.

[61] J.L. Brédas, J.Cornil, D. Beljonne, D.A. Dos Santos, Z. Shuai, Excited-State Electronic Structure of Conjugated Oligomers and Polymers: A Quantum-Chemical Approach to Optical Phenomena, Accounts of Chemical Research (1999) pp. 267-76.

[62] L. C. Kimerling, Band and Bonds, Massachusetts Institute of Technology, Open Online Courses, Materials science and engineering, Photonic materials and devices (2006).

[63] S. Roth, D.Carroll, One-Dimensional Metals, Second Edition, Chapter 5 Conducting Polymers: Solitons and Polarons, WILEY-VCH Verlag GmbH & Co. KGaA, Weinheim (2004) ISBN: 3-527-30749-4.

[64] J.L. Bredas, G.B. Street, Polarons, bipolarons, and solitons in conducting polymers, Accounts of Chemical Research (1985) pp. 309-15.

[65] Wiki, Molecular Models For Organic Lectures, Conducting Polymers (2003).

[66] Springer, Conjugated Conducting Polymers, Dr. Helmut G. Kiess (1992) ISBN:978-3-642-46731-8.

[67] Polymer Electronics, M. Geoghegan, G. Hadziioannou, Oxford University Press (2013) pp. 272.

[68] S. Roth, Introduction to the Physics of Conducting Polymers, Materials Science Forum (1987) pp.1-12.

[69] Shin, J., M. Kim, J. Lee, D. Sin, H. Gyu Kim, H. Hwang, and K. Cho, Effects of conformational symmetry in conjugated side chains on intermolecular packing of conjugated polymers and photovoltaic properties, RSC Adv., (2015) pp.106044-06052.

[70] J.M. Nunzi, Organic photovoltaic materials and devices, Comptes rendus – Physique (2002) pp. 523-542.

[71] N. Li , D. Baran, K. Forberich, F. Machui, T. Ameri, M. Turbiez, M. Carrasco-Orozco, M. Drees, A. Facchetti, F. C. Krebs, C. J. Brabec, Towards 15% energy conversion efficiency: a systematic study of the solution-processed organic tandem solar cells based on commercially available materials, Energy & Environmental Science (2013) pp.3407.

[72] P. Khlyabich, B. Burkhart, B. C. Thompson, Compositional Dependence of the Open-Circuit Voltage in Ternary Blend Bulk Heterojunction Solar Cells Based on Two Donor Polymers, Journal of the American Chemical Society (2012) pp. 9074-077.

[73] P. Cheng, C. Yan, Y. Li, W. Ma, X. Zhan, Diluting concentrated solution: a general, simple and effective approach to enhance efficiency of polymer solar cells, Energy Environmental Science (2015) pp.2357-364.

[74] Z. He, C. Zhong, X. Huang, W.Y. Wong, H. Wu, L. Chen, S. Su, Y. Cao, Simultaneous Enhancement of Open-Circuit Voltage, Short-Circuit Current Density, and Fill Factor in Polymer Solar Cells, Advanced Materials (2011) pp.4636–4643.

[75] Z. A. Page, Y. Liu, V. V. Duzhko, T. P. Russell, T. Emrick, Fulleropyrrolidine interlayers lower cathode work function to raise organic solar cell efficiency, Science (2014) pp.441–444 .

[76] Z. He, B. Xiao, F. Liu, H. Wu, Y. Yang, S. Xiao, C. Wang, T. P. Russell, Y. Cao, Single-junction polymer solar cells with high efficiency and photovoltage, Nature Photonics (2015) pp.174–179.

[77] J. Huang, J. H. Carpenter, C.-Z. Li, J.-S. Yu, H. Ade, A. K. Y. Jen, Highly Efficient Organic Solar Cells with Improved Vertical Donor–Acceptor Compositional Gradient Via an Inverted Off-Center Spinning Method, Advanced Materials (2016) pp.967–974.

[78] A. R. B. M. Yusoff, D. Kim, H. P. Kim, F. K. Shneider, W. J. da Silva, J. Jang, Au-doped single layer graphene nanoribbons for a record-high efficiency ITO-free tandem polymer solar cell, Energy Environmental Science (2015) pp.303–316.

[79] P.Cheng, X. Zhan, Stability of organic solar cells: challenges and strategies, Chemical Society Review (2016) pp.2544-582.

[80] F. C. Krebs, K. Norrman, Analysis of the failure mechanism for a stable organic photovoltaic during 10 000 h of testing, Progress in Photovoltaics (2007) pp. 697–712.

[81] A. Sharma, G. Andersson , D. A. Lewis, Role of humidity on indium and tin migration in organic photovoltaic devices, Physical Chemistry Chemical Physics (2011) pp.4381–4387.

[82] S. T. Lee, Z. Q. Gao and L. S. Hung, Metal diffusion from electrodes in organic light-emitting diodes, Applied Physics Letters (1999) pp.1404–1406.

[83] R. Franke, B. Maennig, A. Petrich, M. Pfeiffer, Long-term stability of tandem solar cells containing small organic molecules, Solar Energy Materials and Solar Cells (2008) pp.732–735.

[84] M. Glatthaar, M. Riede, N. Keegan, K. Sylvester-Hvid, B. Zimmermann, M. Niggemann, A. Hinsch, A. Gombert, Efficiency limiting factors of organic bulk heterojunction solar cells

identified by electrical impedance spectroscopy, Solar Energy Materials and Solar Cells (2007) pp.390–393.

[85] M. O. Reese, A. M. Nardes, B. L. Rupert, R. E. Larsen, D. C. Olson, M. T. Lloyd, S. E. Shaheen, D. S. Ginley, G. Rumbles and N. Kopidakis, Photoinduced degradation of polymer and polymer-fullerene active layers: Experiment and theory, Advanced Functional Materials (2010) pp.3476–3483.

[86] J. Schafferhans, A. Baumann, A. Wagenpfahl, C. Deibel and V. Dyakonov, Oxygen doping of P3HT:PCBM blends: Influence on trap states, charge carrier mobility and solar cell performance, Organic Electronics (2010) pp.1693–1700.

[87] K. Norrman, S. A. Gevorgyan and F. C. Krebs, Water-induced degradation of polymer solar cells studied by H2(18)O labeling , ACS Applied Materials and Interfaces (2009) pp. 102–112.

[88] S. Züfle, M. T. Neukom, S. Altazin, M. Zinggeler, M. Chrapa, T. Offermans and B. Ruhstaller, An Effective Area Approach to Model Lateral Degradation in Organic Solar Cells, Advanced Energy Materials (2015) pp.1500835.

[89] F. C. Krebs, S. A. Gevorgyan, J. Alstrup, A roll-to-roll process to flexible polymer solar cells: model studies, manufacture and operational stability studies, Journal of Materials Chemistry (2009) pp.5442–5451.

[90] L. Córcoles, J. Abad, J. Padilla, A. Urbina, Wavelength influence on the photodegradation of P3HT:PCBM organic solar cells, Solar Energy Materials and Solar Cells (2015) pp. 423–428.

[91] M. V. Madsen, T. Tromholt, K. Norrman, F. C. Krebs, Concentrated light for accelerated photo degradation of polymer materials, Advanced Energy Materials (2013) pp.424–427.

[92] S. Chambon, A. Rivaton, J.-L. Gardette and M. Firon, Photo- and thermo-oxidation of poly(p-phenylene-vinylene) and phenylene-vinylene oligomer, Polymer Degradation and Stability (2011) pp. 1149–1158.

[93] A. Rivaton, S. Chambon, M. Manceau, J.-L. Gardette, N. Lemaître and S. Guillerez, Light-induced degradation of the active layer of polymer-based solar cells, Polymer Degradation and Stability (2010) pp.278–284.

[94] M. Manceau, A. Rivaton, J.-L. Gardette, S. Guillerez and N. Lemaître, The mechanism of photo- and thermooxidation of poly(3-hexylthiophene) (P3HT) reconsidered, Polymer Degradation and Stability (2009) pp. 898–907.

[95] A. Manor, E. A. Katz, T. Tromholt and F. C. Krebs, Electrical and Photo-Induced Degradation of ZnO Layers in Organic Photovoltaics, Advanced Energy Materials (2011) pp.836–843.

[96] G. Williams, Q. Wang and H. Aziz, The Photo-Stability of Polymer Solar Cells: Contact Photo-Degradation and the Benefits of Interfacial Layers, Advanced Functional Materials (2013) pp.2239–2247.

[97] F. Deschler, A. De Sio, E. von Hauff, P. Kutka, T. Sauermann, H.-J. Egelhaaf, J. Hauch and E. Da Como, The effect of ageing on exciton dynamics, charge separation, and recombination in P3HT/PCBM photovoltaic blends, Advanced Functional Materials (2012) pp. 1461-1469.

[98] C. H. Peters, I. T. Sachs-Quintana, W. R. Mateker, T. Heumueller, J. Rivnay, R. Noriega, Z. M. Beiley, E. T. Hoke, A. Salleo and M. D. McGehee, The Mechanism of Burn-in Loss in a High Efficiency Polymer Solar Cell, Advanced Materials (2012) pp.663–668.

[99] U. Aygül, H. Hintz, H.-J. Egelhaaf, A. Distler, S. Abb, H. Peisert and T. Chassé, Energy Level Alignment of a P3HT/Fullerene Blend during the Initial Steps of Degradation, Journal of Physical Chemistry C (2013) pp.4992–4998.

[100] A. Aguirre, S. C. J. Meskers, R. A. J. Janssen and H. J. Egelhaaf, Formation of metastable charges as a first step in photoinduced degradation in π-conjugated polymer:fullerene blends for photovoltaic applications, Organic Electronics (2011) pp.1657–1662.

[101] A. J. Pearson, T. Wang, R. A. L. Jones, D. G. Lidzey, P. A. Staniec, P. E. Hopkinson and A. M. Donald, Rationalizing Phase Transitions with Thermal Annealing Temperatures for P3HT:PCBM Organic Photovoltaic Devices, Macromolecules (2012) pp.1499–1508.

[102] S. R. Dupont, F. Novoa, E. Voroshazi and R. H. Dauskardt, Decohesion Kinetics of PEDOT:PSS Conducting Polymer Films, Advanced Functional Materials (2014) pp.1325–1332.

[103] C. Bruner, F. Novoa, S. Dupont and R. Dauskardt, Decohesion Kinetics in Polymer Organic Solar Cells, ACS Applied Materials and Interfaces (2014) pp.21474–21483.

[104] M.G. Loudon, Chemistry of Naphthalene and the Aromatic Heterocycles, Organic Chemistry (4th ed.), New York: Oxford University Press. (2002) pp. 1135–1136 ISBN 0-19-511999-1.

[105] D. L. Wise, G. E. Winek, D. J. Trantolo, T. M. Cooper, J. D. Gresser, Electrical and Optical Polymer Systems, vol.17, Marcel Dekker, Inc., New York (1998).

[106] J. Rodriguez, H. J. Grande, T. F. Otero, Handbook of Organic Conductive Molecules and Polymers, ed. H. S. Nalwa, John Wiley & Sons, New York, (1997).

[107] J. Simonet, J. R. Berthelot, Electrochemistry : a technique to form, to modify and to characterize organic conducting polymers, Progress in Solid State Chemistry (1991) vol. 21, pp.1.

[108] N.N. Zhou, H.T. Zhu, D.S. Yang, Z.H. Guan, Recent developments in the group-1B-metal-catalyzed synthesis of pyrroles. Organic and Biomolecular Chemistry (2016) pp.7136–7149.

[109] P.He, Q. Xiao-Lan, Q. Qun, L.Hong-Xiang, Thieno[3,4-c]pyrrole-4,6-dione based copolymers for high performance organic solar cells and organic field effect transistors, Chinese Chemical Letters (2016) pp. 1277-282.

[110] S. G. Somnath, Pyrrole: An emerging scaffold for construction of valuable therapeutic agents, European Journal of Medicinal Chemistry (2016) pp.13-31.

[111] J. Heinze, Electronically Conducting Polymers, Topics in Current Chemistry (1990).

[112] Y.-J. Qiu, J R. Reynolds,Electrochemically initiated chain polymerization of pyrrole in aqueous media, Journal of Polymer Science Part A: Polymer Chemistry (1992) pp.1315-325.

[113] K. J. Kim, H. S. Song, J. D. Kim, Mechanism of electropolymerization of pyrrole in acidic aqueous solutions, Bull. Korean Chemical Society (1988) pp.248.

[114] S. Asavapiriyanont, G. K. Chandler, G. A. Gunawardena, D. Pletcher, The electrodeposition of polypyrrole films from aqueous solutions, The Journal of electroanalytical chemistry and interfacial electrochemistry (1984) pp. 229.

[115] B. L. Funt and A. F. Diaz, Organic Electrochemistry: an Introduction and a Guide, Marcel Dekker, New York (1991) pp.1337.

[116] A. F. Diaz, E. M. Genies, G. Bidan, Spectroelectrochemical study of polypyrrole films, Journal of Electroanalytical Chemistry and Interfacial Electrochemistry (1983) pp.149(1-2).

[117] R. J. Waltman, J. Bargon, Electrically conducting polymers: a review of the electropolymerization reaction, of the effects of chemical structure on polymer film properties, and of applications towards technology, Canadian Journal of Chemistry (1986) pp.76-95.

[118] R. J. Waltman, J. Bargon, Reactivity/structure correlations for the electropolymerization of pyrrole: An INDO/CNDO study of the reactive sites of oligomeric radical cations, Tetrahedron (1984) pp.3963-3970.

[119] S. Sadki, P. Schottland, N. Brodie, G. Sabouraud, The Mechanisms of Pyrrole Electropolymerization, ChemInform (2000) pp.51.

[120] S. Sadki, P. Schottland, N. Brodie, G. Sabouraud, The Mechanisms of Pyrrole Electropolymerization, (Review Article) Chemical Society Reviews (2000) pp.283-293.

[121] M.M. Ayad, Influence of HCL on polypyrrole films prepared chemically from ferric chloride, Journal of Polymer Chemistry (1994) pp.9–14.

[122] F. Ferrero, L. Napoli, C. Tonin, A. Varesano, Pyrrole chemical polymerization on textiles: Kinetics and operating conditions, Journal of Applied Polymer Science (2006) pp.4121–4126.

[123] Y. Tan, K. Ghandi, Kinetics and mechanism of pyrrole chemical polymerization, Synthetic Metals (2013) pp.183–191.

[124] S. Paul, Polypyrrole Formation and Use, Defence Research and Development Canada, Technical Memorandum (2005).

[125] L. M. M Mithra,. Y. Cao, S. Cho, D. Sutar, K. Lee, R. Menon, S.V. Subramanyam, Electrical transport and reflectance studies on polypyrrole- CF3SO3- in the vicinity of metal-insulator transition, Synthetic Metals (2001) pp.437.

[126] C. Janáky, C. Wilaiwan, R. Krishnan, Mechanistic Aspects of Photoelectrochemical Polymerization of Polypyrrole on a TiO2 Nanotube Array, Electrochimica Acta (2014) pp.303-09.

[127] C. Janaky, N. de Tacconi, W. Chanmanee, K. Rajeshwar, Conjugated Polymers and Oxide Nanoarchitectures into Intimate Contact: Light Induced Electrodeposition of Polypyrrole and Polyaniline on Nanoporous WO_3 or TiO_2, Journal of Physical Chemistry C, (2012) pp.19145–19155.

[128] Mitsutoshi Okano, Kiminori Itoh, and Akira Fujishima, Photoelectrochemical Polymerization of Pyrrole on Ti02 and Its Application to Conducting Pattern Generation, J. Electrochem. Soc.: ELECTROCHEMICAL SCIENCE AND TECHNOLOGY (1987) pp.837-841.

[129] C. Janáky, K. Rajeshwar, The role of (photo)electrochemistry in the rational design of hybrid conducting polymer/semiconductor assemblies: From fundamental concepts to practical applications, Progress in Polymer Science (2015) pp.96-135.

[130] M.A. Fox, K.L. Worthen, Comparison of the physical properties of polypyrrole produced by anodic oxidation and by photoelectrochemical activation of TiO_2, Chemistry of Materials (1991) pp. 253–257.

[131] A. Jarkov, S. Bereznev, O. Volobujeva, R. Traksmaa, A. Tverjanovich, A. Öpik, E. Mellikov Photo-assisted electrodeposition of polypyrrole back contact to CdS/CdTe solar cell structures, Thin Solid Films (2013) pp.198–201.

[132] A. Ramanavicius, V. Karabanovas, A. Ramanaviciene, R. Rotomskis, Stabilization of (CdSe)ZnS quantum dots with polypyrrole formed by UV/Vis irradiation initiated polymerization Journal of Nanoscience and Nanotechnology (2009) pp.1909–1915.

[133] F. Goubard, P.H. Aubert, K. Boukerma, E. Pauthe, C. Chevrot, Elaboration of nanohybrid materials by photopolymerisation of 3,4-ethylenedioxythiophene on TiO_2, Chemical Communications (2008) pp.3139–3141.

[134] Y.S. Abé, L.M. Ugalde, D.V. Angélica, Y.Trégouët, J. C. Bernède, Nucleation and growth mechanism of polycarbazole deposited by electrochemistry, Journal of the Brazilian Chemical Society (2007) pp.601-06.

[135] R. Schrebler, , P. Grez, P. Cury, C. Veas, M. Merino, H. Gómez, R. Córdova, M.a. Del Valle, Nucleation and growth mechanisms of poly(thiophene) Part 1. Effect of electrolyte and monomer concentration in dichloromethane, Journal of Electroanalytical Chemistry (1997) pp. 77-90.

[136] M. Romero, M. A. del Valle, R. del Río, F. R. Díaz, F. Armijo Polymers Nucleation and Growth Mechanism: Solubility, a Determining Factor, Int. J. Electrochem. Sci., (2012) pp.10132 – 10141.

[137] M.A. del Valle, F.R. Díaz, M.E. Bodini, G. Alfonso, G.M. Soto, E. E. Borrego, Electrosynthesis and characterization of o-phenylenediamine oligomers, Polymer International (2005) pp.526–532.

[138] R. Córdova, M.A. del Valle, A. Arratia, H. Gómez, R. Schreble, Effect of anions on the nucleation and growth mechanism of polyaniline, Journal of Electroanalytical Chemistry (1994) pp.75-83.

[139] M.A del Vallea, P Curyb, R. Schrebler, Solvent effect on the nucleation and growth mechanisms of poly(thiophene), Electrochimica Acta (2002) pp.397–405.

[140] T. Xu, Q. Qiao, Conjugated polymer–inorganic semiconductor hybrid solar cells, Energy & Environmental Science (2011) pp.2700–2720.

[141] S. Ren, L.-Y. Chang, S.-K. Lim, J. Zhao, M. Smith, N. Zhao, V. Bulovic, M. Bawendi, S. Gradečak, Inorganic–Organic hybrid solar cell: bridging quantum dots to conjugated polymer nanowires, Nano Letters (2011) pp.3998–4002.

[142] M. Wright, U, Ashraf Uddin, Organic—inorganic hybrid solar cells: A comparative review, Solar Energy Materials and Solar Cells (2012) pp.87-111.

[143] D. Celik, M. Krueger, C. Veit, H.F. Schleiermacher, B. Zimmermann, S. Allard, I. Dumsch, U. Scherf, F. Rauscher, P. Niyamakom, Performance enhancement of CdSe nanorod-polymer based hybrid solar cells utilizing a novel combination of post-synthetic nanoparticle surface treatments, Solar Energy Materials and Solar Cells (2012) pp.433–440.

[144] S. Dayal, N. Kopidakis, D.C. Olson, D.S. Ginley, G. Rumbles, Photovoltaic devices with a low band Gap polymer and CdSe nanostructures exceeding 3% efficiency, Nano Letters, 10 (2009) pp.239–242.

[145] A. Guchhait, A.K. Rath, A.J. Pal, To make polymer: quantum dot hybrid solar cells NIR-active by increasing diameter of PbSnanoparticles, Solar Energy Materials and Solar Cells (2011) pp.651–656.

[146] I. Gonzalez-Valls, M. Lira-Cantu, Vertically-aligned nanostructures of ZnO for excitonic solar cells: a review, Energy & Environmental Science (2009) pp.19–34.

[147] S.R. Brian, Hybrid polymer/nanoparticle solar cells: preparation, principles and challenges, Journal of Colloid and Interface Science (2012) pp.1–15.

[148] X. Yang, J. Loos, S.C. Veenstra, W.J.H. Verhees, M.M. Wienk, J.M. Kroon, M.A.J. Michels, R.A.J. Janssen, Nanoscale morphology of high-performance polymer solar cells, Nano Letters (2005) pp.579–583.

[149] M.T. Dang, G. Wantz, H. Bejbouji, M. Urien, O.J. Dautel, L. Vignau, L. Hirsch, Polymeric solar cells based on P3HT:PCBM: role of the casting solvent, Solar Energy Materials and Solar Cells (2011) pp.3408–3418.

[150] L. Chang, H.W.A. Lademann, J.-B. Bonekamp, K. Meerholz, A.J. Moulé, Effect of trace solvent on the morphology of P3HT:PCBM bulk heterojunction solar cells, Advanced Functional Materials (2011) pp.1779–1787.

[151] Z. He, C. Zhong, X. Huang, W.-Y. Wong, H. Wu, L. Chen, S. Su, Y. Cao, Simultaneous enhancement of open-circuit voltage, short-circuit current density, and fill factor in polymer solar cells, Advanced Materials (2011) pp.4636–4643.

[152] Y. Liang, Z. Xu, J. Xia, S.-T. Tsai, Y. Wu, G. Li, C. Ray, L. Yu, For the bright future—bulk heterojunction polymer solar cells with power conversion efficiency of 7.4%, Advanced Materials (2010) pp.E135–E138.

[153] M. Helgesen, R. Sondergaard, F.C. Krebs, Advanced materials and processes for polymer solar cell devices, Journal of Materials Chemistry (2010).

[154] H. Borchert, Elementary processes and limiting factors in hybrid polymer/nanoparticle solar cells, Energy & Environmental Science (2010) pp.1682–1694.

[155] D. Celik, M. Krueger, C. Veit, H.F. Schleiermacher, B. Zimmermann, S. Allard, I. Dumsch, U. Scherf, F. Rauscher, P. Niyamakom, Performance enhancement of CdSe nanorod-polymer based hybrid solar cells utilizing a novel combination of post-synthetic nanoparticle surface treatments, Solar Energy Materials and Solar Cells (2012) pp.433–440.

[156] S. Ren, L.-Y. Chang, S.-K. Lim, J. Zhao, M. Smith, N. Zhao, V. Bulovic, M. Bawendi, S. Gradečak, Inorganic–Organic hybrid solar cell: bridging quantum dots to conjugated polymer nanowires, Nano Letters (2011) pp.3998–4002.

[157] H.-C. Chen, C.-W. Lai, I.C. Wu, H.-R. Pan, I.W.P. Chen, Y.-K. Peng, C.-L. Liu, C.-h. Chen, P.-T. Chou, Enhanced performance and air stability of 3.2% hybrid solar cells: how the functional polymer and CdTe nanostructure boost the solar cell efficiency, Advanced Materials (2011) pp.5451–5455.

[158] C.-Y. Liu, Z.C. Holman, U.R. Kortshagen, Optimization of Si NC/P3HT hybrid solar cells, Advanced Functional Materials (2010) pp.2157–2164.

[159] A. Guchhait, A.K. Rath, A.J. Pal, To make polymer: quantum dot hybrid solar cells NIR-active by increasing diameter of PbSnanoparticles, Solar Energy Materials and Solar Cells (2011) pp.651–656.

[160] T. Krishnamoorthy, V. Thavasi, M. Subodh, G, S. Ramakrishna, A first report on the fabrication of vertically aligned anatase TiO2 nanowires by electrospinning: preferred architecture for nanostructured solar cells, Energy & Environmental Science (2011).

[161] S.D. Oosterhout, M.M. Wienk, S.S. van Bavel, R. Thiedmann, L. Jan Anton Koster, J. Gilot, J. Loos, V. Schmidt, R.A.J. Janssen, The effect of three-dimensional morphology on the efficiency of hybrid polymer solar cells, Nature Materials (2009) pp.818–824.

[162] [M. Bredol, K. Matras, A. Szatkowski, J. Sanetra, A. Prodi-Schwab, P3HT/ZnS: a new hybrid bulk heterojunction photovoltaic system with very high open circuit voltage, Solar Energy Materials and Solar Cells (2009) pp.662–666.

[163] G. Kumar, V. Mohan, Raman, Jin Kawakita, P. Ilanchezhiyan, R. Jayavel, Fabrication of polypyrrole/ZnCoO nanohybrid systems for solar cell applications, Dalton Transactions (2010) pp.8325.

[164] H.Yoneyama, K. Wakamoto, H. Tamura, Photo-assisted electrochromic behavior of polyaniline and polypyrrole films coated on platinized n-type silicon, Materials Chemistry and Physics (1986) pp.567-75.

[165] A. Neumüller, S. Bereznev, M. Ewert, O. Volobujeva, O. Sergeev, J. Falta, M. Vehse, and C. Agert, Carrier collection losses in interface passivated amorphous silicon thin-film solar cells, Applied Physics Letters (2016) pp. 109(4):043903.

[166] Libretexts. "Cyclic Voltammetry, Chemistry LibreTexts (2017) Accessed May 2017.

[167] H. Gerischer, Photoassisted interfacial electron transfer, Surf. Sci. (1980) pp.518–530.

[168] Mcneill, C. R., I. Hwang, and N. C. Greenham, Photocurrent transients in all-polymer solar cells: Trapping and detrapping effects, Journal of Applied Physics (2009) pp.024507.

[169] "Transient photocurrent." Wikipedia (2016) Accessed May 2017.

[170] "Scanning electron microscope." Wikipedia (2017) Accessed May 2017.

[171] V. Saini, O. Abdulrazzaq, S. Bourdo, E. Dervishi, A. Petre, V. Gopal Bairi, T. Mustafa, L. Schnackenberg, T. Viswanathan and A. S. Biris, Structural and optoelectronic properties of P3HT-graphene composites prepared by in situ oxidative polymerization, Journal of Applied Physics (2012) pp.054327.

[172] "Ultraviolet–visible spectroscopy" Wikipedia. (2017) Accessed May 2017.

[173] Madsen, Morten V., UV-vis spectroscopy (2017).

[174] "Kelvin probe force microscope" Wikipedia. (2017) Accessed May 2017.

[175] L. Cheran, S. Sadeghi, M. Thompson, Scanning Kelvin nanoprobe detection in materials science and biochemical analysis, The Analyst (2005) pp.1569.

[176] KP Technology Ltd. Accessed May 2017.

[177] "I-V Curve", PV Education, Accessed May 2017.

[178] A. Almario, R.L. Vieira, Study Of Polypyrrole Films Modified With Copper And Silver Microparticles By Electrochemical Cementation Process, Journal of the Chilean Chemical Society, (2006) 51(3).

[179] A. Tabchouche, A. Ourari, N. Zoubeidi, D. Zerrouki, Electrochemistry Preparation of Electrodes based on Polypyrrole and polymethylpyrrole/Manganese Dioxide Particles, Energy Procedia, 36 (2013) pp. 1009-1017.

[180] G.B. Street, T.C. Clarke, R.H. Geiss, V.Y. Lee, A. Nazzal, P. Pfluger, J.C. Scott, Characterization Of Polypyrrole, Le Journal de Physique Colloques (1983) C3.

[181] R. Kiefer, D.G. Weis, A. Aabloo, G. Urban, J. Heinze, Dependence of polypyrrole bilayer deflection upon polymerization potential, Synthetic Metals (2013) pp. 37-43.

[182] S. Asavapiriyanont, G. Chandler, G. Gunawardena, D. Pletcher, The electrodeposition of polypyrrole films from aqueous solutions, Journal of Electroanalytical Chemistry and Interfacial Electrochemistry (1984) pp.229-244.

[183] C. Debiemme-Chouvy, T.T. Tran, An insight into the overoxidation of polypyrrole materials, Electrochemistry Communications (2008) pp.947-950.

[184] S. Bereznev, I. Konovalov, A. Öpik, J. Kois, E. Mellikov, Hybrid copper–indium disulfide/polypyrrole photovoltaic structures prepared by electrodeposition, Solar Energy Materials and Solar Cells (2005) pp.197-206.

[185] S. Asavapiriyanont, G. Chandler, G. Gunawardena, D. Pletcher, The electrodeposition of polypyrrole films from aqueous solutions, Journal of Electroanalytical Chemistry and Interfacial Electrochemistry (1984) pp.229-244.

[186] M.A. Fox, R. Akaba, Curve crossing in the cyclic voltammetric oxidation of 2-phenylnorbornene. Evidence for an ECE reaction pathway, Journal of the American Chemical Society (1983) pp.3460-3463.

[187] A. Almario, R.L. Vieira, Study Of Polypyrrole Films Modified With Copper And Silver Microparticles By Electrochemical Cementation Process, Journal of the Chilean Chemical Society, 51(3) (2006).

[188] V. G. Dubrovskii, Nucleation Theory and Growth of Nanostructures,1, NanoScience and Technology (2014) pp:20, Springer-Verlag Berlin Heidelberg.

[189] C. Pirvu, M. Mindroiu, I. Demetrescu, One-Step Potentiostatic Electrodeposition of Polypyrrole Coatings on Zinc Coated Steel Surfaces, Key Engineering Materials (2009) pp. 65-68.

[190] S. Bereznev, I. Konovalov, A. Öpik, J. Kois, E. Mellikov, Hybrid copper–indium disulfide/polypyrrole photovoltaic structures prepared by electrodeposition, Solar Energy Materials and Solar Cells (2005) pp.197-206.

[191] F. Demichelis, C. F. Pirri, and E. Tresso, Influence of doping on the structural and optoelectronic properties of amorphous and microcrystalline silicon carbide, Journal of Applied Physics (1992) pp.1327-333.

[192] Y. Zhang, C. Yu, M. Yang, Y. He, L. Zhang, J. Zhang, X. Xu, Y. Zhang, X. Song, and H. Yan, Optimization of the window layer in large area silicon heterojunction solar cells, RSC Adv.,(2017) pp.9258-263.

[193] Yang, R., W. H. Smyrl, D. F. Evans, W. A. Hendrickson, Evolution of polypyrrole band structure: a scanning tunneling spectroscopy study, The Journal of Physical Chemistry (1992) pp.1428-1430.

[194] Čabala, R., J. Škarda, K. Potje-Kamloth, Spectroscopic investigation of thermal treatment of doped polypyrrole, Physical Chemistry Chemical Physics (2000) pp.3283-3291.

[195] Nayak, J., S. K. Mahadeva, J. Kim, Characteristics of flexible electrode made on cellulose by soluble polypyrrole coating, Proceedings of the Institution of Mechanical Engineers, Part C: Journal of Mechanical Engineering Science (2012) pp.2605-2609.

[196] Brédas, J. L., B. Thémans, J. M. André, Bipolarons in polypyrrole chains, Physical Review B (1983) pp.7827-830.

[197] W. Tress, K. Leo, M. Riede, Influence of Hole-Transport Layers and Donor Materials on Open-Circuit Voltage and Shape of I-V Curves of Organic Solar Cells, Advanced Functional Materials (2011) pp.2140–2149.

[198] A. Kumar, S. Sista, Y. Yang, Dipole induced anomalous S-shape I-V curves in polymer solar cells, Journal of Applied Physics (2009) pp.094512.

[199] W.Tress, O.Inganäs. Simple experimental test to distinguish extraction and injection barriers at the electrodes of (organic) solar cells with S-shaped current–voltage characteristics, Solar Energy Materials and Solar Cells (2013) pp.599-603.

[200] A.Kumar, S Srinivas, Y.Yang, Dipole induced anomalous S-shape I-V curves in polymer solar cells, Journal of Applied Physics (2009) pp.094512.

[201] R. Saive, C.Mueller, J. Schinke, R. Lovrincic, W. Kowalsky,Understanding S-shaped current-voltage characteristics of organic solar cells: Direct measurement of potential distributions by scanning Kelvin probe, Applied Physics Letters (2013) pp.243303.

[202] Z. Alparslan, A. Kösemen, O. Örnek, Y. Yerli, and S. Eren San,TiO_2-Based Organic Hybrid Solar Cells with Mn^{+2} Doping, International Journal of Photoenergy (2011) pp.1-8.

[203] Institute for Microelectronics, Quantum Mechanical Tunneling, Accessed May (2017).

Appendix I

This work is based on an article that was accepted and published in the Materials Science in Semiconductor Processing journal:

D. Dosenovicova, J. Maricheva, A. Neumüller, O. Sergeev, O. Volobujeva, A.G. Nasibulin, J. Kois, A. Öpik, S. Bereznev, *Selective photoelectrochemical deposition of polypyrrole onto hydrogenated a-Si for optoelectronic applications*, Materials Science in Semiconductor Processing 68 (2017) 1-5.

Additionally, this work was presented at the following conferences:

1. The Baltic Polymer Symposium (2016) with a presentation entitled: *'' Hybrid solar cells based on a-Si and electrodeposited''*, Klaipeda University Aula Magna conference complex, Kaunas University of Technology, Kaunas, Lithuania.
2. Open Readings (2017) with a poster entitled: *'' Photoelectrochemical deposition of PPY onto hydrogenated A-SI for optoelectronic applications''*, Ed. Vilnius University. Vilnius, Lithuania.